Research Paper
Computational Methods for Differential Equations
http://cmde.tabrizu.ac.ir
Vol. *, No. *, *, pp. 1-32
DOI:10.22034/cmde.2026.70032.3460

Optimal control and mathematical modeling of COVID-19 dynamics: Insights from Iran

Hossein Gholami Chahkand[1], **Mortaza Gachpazan**[1,*], **and Majid Erfanian**[2,*]
[1]Department of Applied Mathematics, School of Mathematical Sciences, Ferdowsi University of Mashhad, Mashhad, Iran.
[2]Department of Mathematics, Faculty of Science, University of Zabol, Zabol, Iran.

Abstract

In this paper, we propose a mathematical model for the transmission of coronavirus-19 disease (COVID-19) to understand under which conditions it will be eradicated or persisted. The dynamics of COVID-19 for this study is divided into seven classes: susceptible, vaccinated, exposed, symptomatically infected, asymptomatically infected, quarantined, and recovered. The model has both disease-free and endemic equilibria. The basic reproduction number ($\mathcal{R}_0$) is computed using the next-generation matrix method. It is shown that the disease-free equilibrium is both locally and globally asymptotically stable, whereas the endemic equilibrium is proved to be only locally asymptotically stable. From March 31, 2020, to July 31, 2021, Iran experienced four waves of COVID-19. The observed monthly cumulative cases were approximated by quadratic polynomials, and their shapes were evaluated for consistency with the qualitative dynamics predicted by the model. We have formulated and solved an optimal control problem to understand the effects of performance of vaccination of susceptible individuals and treatment of quarantined individuals to hinder the outbreak of this illness. Finally, sensitivity analysis and numerical simulations confirmed that the implementation of quarantine, vaccination, and putting on face masks will help to minimize the spread of the COVID-19 virus.

Keywords. Basic reproduction number, Equilibria, Stability, Optimal control, Sensitivity analysis.
2010 Mathematics Subject Classification. 92B05, 92D25, 92D30, 37N25, 34D23.

1. Introduction

Coronavirus is a kind of disease that is caused by an infection in the respiratory system of birds and mammals [**?**]. Coronaviruses were discovered in the 1960 decade, and study of them kept on continuously until the mid-1980s [**?** **?**]. The latest type of coronavirus, the severe acute respiratory syndrome coronavirus-2 (SARS-CoV-2) broke out in December 2019 in Wuhan, China, with an epidemic in humans. After a short period of time, it became an international crisis. These viruses have a core of genetic material and a membrane full of protein spikes. In fact, the appearance of these viruses is very similar to a crown. The crown is the corona in Latin. Coronavirus often causes problems in the respiratory and gastrointestinal systems.
Sometimes, this virus can be transmitted from animals to humans. The phenomenon of virus transmission from animal to human is called spillover. The reason for spillover can be a wide range of factors, such as genetic changes in the virus or increased contact between humans and animals; for example, Middle East Respiratory syndrome coronavirus disease (MERS-CoV), which is transmitted from camels, and SARS-CoV, which is transmitted from domestic cats. SARS-CoV-2 like the MERS and SARS coronaviruses, likely evolved from a virus previously found in animals. Assessment of the clinical and epidemiological characteristics of SARS-CoV-2 cases suggests that patients will not be infectious until the onset of symptoms. In most cases, individuals are usually considered infectious while they have symptoms; how infectious individuals are, depends on the severity of their symptoms and stage of their illness. SARS-CoV-2 is the virus responsible for the 2019 outbreak of COVID-19 disease. COVID-19 (COrona VIrus Disease 2019) has affected the lives of people all over the world in a surprising way since its appearance. SARS and MERS are older versions of

Received:02 November 2025; Accepted: 01 July 2026.
∗ Corresponding author. Email: gachpazan@um.ac.ir, erfaniyan@uoz.ac.ir.

coronavirus. More than 200 types of coronavirus are known. The number of coronaviruses that have been known so far is only the tip of the iceberg, and a large and unknown part of them have the potential to cause new and severe events for animals and humans.

In order to minimize the dissemination of COVID-19 world wide, different strategies have been employed. Obligation to wear face masks in crowded areas, washing hands, disinfecting surfaces, limitation of number of people in public transport, quarantine, continuous vaccination etc are some examples of these strategies.

Mathematical models are important and beneficial instruments to help humans understand how the dynamics of a disease spread in a population. Mathematical models play an important role in predicting the biological and physical behavior of diseases. For example, in predicting the spread of diseases [**?** **?**], investigating the effects of variable factors such as control measures [**?**], designing and evaluating various policies such as quarantine and population vaccination [**?**], predicting the temporal changes of disease and manufacturing experimental models are used to evaluate the possible effects of drugs and other treatments [**?**]. Previously, many researchers have used mathematical models to explain and describe various diseases. Yan et al. [**?**] used it to describe their SARS transmission model. Also, Jung et al. [**?**] applied a system of ordinary differential equations for modeling two-strain tuberculosis. Agusto et al. [**?**] presented a deterministic system of differential equations for the transmission of malaria. Furthermore, Agusto and Ogunye [**?**] presented an application of optimal control theory for modeling avian influenza transmission dynamics in birds. Bowman et al. [**?**] explored West Nile Virus (WNV) and proposed a single-season ordinary differential equation model for the transmission dynamics of WNV in a mosquito-bird-human community.

Deterministic compartmental models are a type of mathematical model used to model disease transmission and population changes. These models use the partition of the population into different classes, and ordinary differential equations are usually used to describe the temporal changes in each class. For example, Parsamanesh and Erfanian [**?**] constructed a susceptible-infected-vaccination model by considering a vaccination program efficacy for new members and susceptible individuals. Alqahtani [**?**] constructed the susceptible-infectious-removed model by considering the effect of the health system. In addition, interested readers can see the mathematical modeling of other diseases such as dengue fever, Ebola, influenza, HIV/AIDS, typhoid fever, Chikungunya, cancer and Nipah in [**?** **?** **?** **?** **?** **?** **?** **?** **?** **?** **?** **?** **?**] and the references therein.

This paper extends the work of [**?**] by adding the vaccinated class and eliminating the death compartment. The rest of the article is summarized as follows. In section 2, the proposed model is formulated. The positivity and boundedness of solutions are proved in this section. In section 3, the equilibrium points and basic reproduction number for the model are obtained. In section 4, we present stability analysis for the equilibrium points. Curves fitting are presented in section 5. Our model has been reformulated as an optimal control problem in section 6. Sensitivity index and numerical analysis are studied in section 7. Finally, conclusion is given in section 8.

2. Model formulation and properties

This model will be constituted dividing into seven compartments of the population. The total size of human population at time t, is denoted by $N(t)$. It comprises the susceptible (S), vaccinated (V), exposed (E), symptomatically infected (I_s), asymptomatically infected (I_a), quarantined (Q), and recovered (R) compartments, such that

$$N(t) = S(t) + V(t) + E(t) + I_s(t) + I_a(t) + Q(t) + R(t), \quad t \geq 0. \tag{2.1}$$

The proposed flow diagram for the transmission dynamics of COVID-19 is exhibited in Figure 1. Model variables and parameters are descripted in Table 1. Since the vaccinations for COVID-19 are available, we have considered a vaccinated class (V) in our model. The susceptible class is increased by the recruitment rate ρ. Susceptible individuals catch virus after having contacts with symptomatically or asymptomatically infective individuals with the size of diminish $\zeta_s = [\beta_s(1-\psi\xi)I_s + \beta_a(1-\psi\xi)I_a]S$. The proportion of individuals who use a face mask is denoted by $0 < \psi \leq 1$. In addition, $0 < \xi \leq 1$ represents the efficacy of face masks. The parameters β_s and β_a represent the effective transmission rates from symptomatic and asymptomatic infected classes, respectively. The susceptible individuals are vaccinated at a rate ν. We also consider that individuals in all classes pass away at a rate μ. The vaccinated individuals loss their immunity with the size of diminish $\zeta_v = (1-\epsilon)\omega[\beta_s(1-\psi\xi)I_s + \beta_a(1-\psi\xi)I_a]V$, where ϵ is the proportion of infection reduction due to vaccination. Moreover, ω indicates the proportion of waning immunity after vaccination. φ is the rate at which those exposed become infected. A proportion $0 < \theta \leq 1$ of exposed individuals

TABLE 1. Description of the model variables and parameters.

Variables/Parameters	Description
$S(t)$	Agent of susceptible individuals at time t
$V(t)$	Agent of vaccinated individuals at time t
$E(t)$	Agent of exposed individuals at time t
$I_a(t)$	Agent of asymptomatically infected individuals at time t
$I_s(t)$	Agent of symptomatically infected individuals at time t
$Q(t)$	Agent of quarantined individuals at time t
$R(t)$	Agent of recovered individuals at time t
N	Total human population
ρ	Rate of recruitment (from birth and immigration)
β_s	The effective transmission rate from symptomatic infected class
ψ	The proportion of individuals who use a face mask
ξ	The efficacy of face masks
β_a	The effective transmission rate from asymptomatic infected class
ν	Vaccination rate
ϵ	Proportion of infection reduction due to vaccination
ω	Proportion of waning immunity after vaccination
φ	Rate at which those exposed become infected
α_a	Exit rate from the asymptomatic infected class
η	The proportion of asymptomatic individuals who have been quarantined
α_s	Exit rate from the symptomatic infected class
σ	The proportion of symptomatic individuals who have been quarantined
λ_q	The recovery rate of individuals in the quarantined class
γ	Rate of reduction of the effect of temporary immunity after the recovery
μ	Natural death rate and disease-induced death rate
ζ_s	The size of diminish from susceptible class to exposed class
ζ_v	The size of diminish from vaccinated class to exposed class
θ	The proportion of exposed individuals show no clinical symptoms after the incubation period

shows no clinical symptoms of COVID-19 at the end of the latent period. The exit rate from the asymptomatic and the symptomatic classes are denoted by α_a and α_s, respectively. A proportion $0 < \eta \leq 1$ of asymptomatic individuals represents the rate of individuals who have been quarantined, and the remaining proportion $1-\eta$ shows the recovery rate for individuals in the I_a compartment. Similarly, a proportion $0 < \sigma \leq 1$ of the symptomatic compartment represents the individuals who have been quarantined, and the remaining proportion $1-\sigma$ shows the recovery rate for individuals in the I_s class. Also, λ_q is the recovery rate of individuals in the quarantined compartment. Finally, the parameter γ represents the rate of the reduction of the effect of temporary immunity after the recovery. The model is mathematically formulated as a system of ordinary differential equations as follows:

$$\begin{aligned}
\frac{dS(t)}{dt} &= \rho - [\beta_s(1-\psi\xi)I_s(t) + \beta_a(1-\psi\xi)I_a(t)]S(t) - (\mu+\nu)S(t),\\
\frac{dV(t)}{dt} &= \nu S(t) + \gamma R(t) - (1-\epsilon)\omega[\beta_s(1-\psi\xi)I_s(t) + \beta_a(1-\psi\xi)I_a(t)]V(t) - \mu V(t),\\
\frac{dE(t)}{dt} &= [\beta_s(1-\psi\xi)I_s(t) + \beta_a(1-\psi\xi)I_a(t)](S(t) + (1-\epsilon)\omega V(t)) - (\mu+\varphi)E(t),\\
\frac{dI_a(t)}{dt} &= \theta\varphi E(t) - (\alpha_a+\mu)I_a(t),
\end{aligned}$$

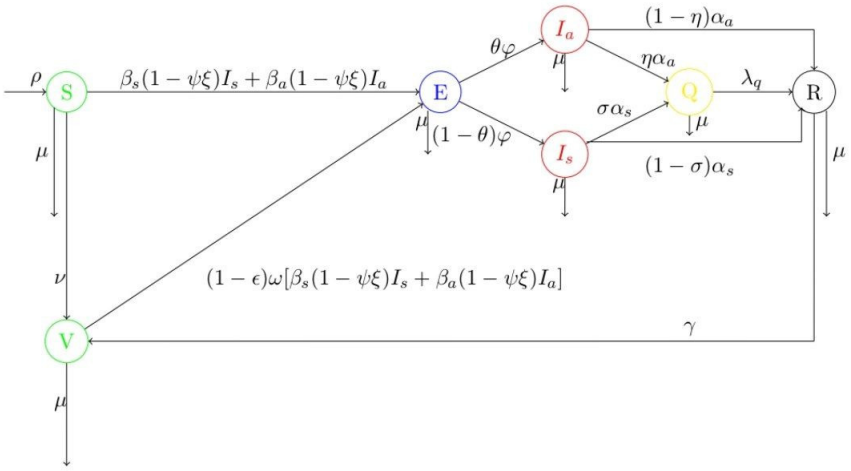

FIGURE 1. The schematic model flow for COVID-19 dynamics.

$$\begin{aligned}
\frac{dI_s(t)}{dt} &= (1-\theta)\varphi E(t) - (\alpha_s+\mu)I_s(t),\\
\frac{dQ(t)}{dt} &= \eta\alpha_a I_a(t) + \sigma\alpha_s I_s(t) - (\lambda_q+\mu)Q(t),\\
\frac{dR(t)}{dt} &= (1-\eta)\alpha_a I_a(t) + (1-\sigma)\alpha_s I_s(t) + \lambda_q Q(t) - (\mu+\gamma)R(t).
\end{aligned} \tag{2.2}$$

From the sum of the equations of model (2.2), we have

$$\frac{dN}{dt} = \rho - \mu N. \tag{2.3}$$

Model dynamics can be considered in the region below:

$$\Omega = \{(S,V,E,I_a,I_s,Q,R) \subset \mathbb{R}_+^7 : N \leq \frac{\rho}{\mu}\}. \tag{2.4}$$

The motivation for including each class in the model is as follows:

- **Susceptible (S):** Individuals at risk of infection. Recruitment increases this class, while infection, vaccination, and natural death decrease it.
- **Vaccinated (V):** Individuals who received vaccination. Vaccination reduces susceptibility, and immunity can wane over time, allowing reinfection.
- **Exposed (E):** Individuals infected but not yet infectious, representing the incubation period.
- **Asymptomatic (I_a) and Symptomatic (I_s) infected:** Infected individuals with or without symptoms. Symptomatic individuals are more likely to be detected and quarantined.
- **Quarantined (Q):** Individuals isolated to prevent transmission.
- **Recovered (R):** Individuals who recovered from infection. Temporary immunity may decrease, transferring some individuals to the vaccinated class V.

It is worth mentioning that we do not explicitly include a deceased class. Disease-induced deaths are assumed to occur at the same rate μ as natural deaths.

2.1. **Positivity and boundedness of solutions.** Since this study includes the human population, it is necessary to examine whether it is biologically feasible. Therefore, we express the following two theorems. The first theorem proves that model solutions are positive.

Theorem 2.1. *Assume nonnegative initial conditions*

$$S(0), V(0), E(0), I_a(0), I_s(0), Q(0), R(0) \geq 0.$$

Then the solution of system (2.2) exists, is unique and satisfies

$$S(t), V(t), E(t), I_a(t), I_s(t), Q(t), R(t) \geq 0 \qquad \text{for all } t \geq 0.$$

Moreover the feasible region

$$\Omega = \{(S, V, E, I_a, I_s, Q, R) \in \mathbb{R}^7_+ : \ N(t) \leq \rho/\mu\},$$

is positively invariant.

Proof. Uniqueness and local existence follow from standard ODE theory because the right-hand sides of (2.2) are locally Lipschitz in $\mathbb{R}^7$. It remains to prove nonnegativity for all $t \geq 0$ and positive invariance of Ω.
(i) Total population bound. Summing the equations in (2.2) gives

$$\frac{dN}{dt} = \rho - \mu N(t),$$

where $N(t) = S + V + E + I_a + I_s + Q + R$. This linear scalar ODE has the explicit solution

$$N(t) = N(0)e^{-\mu t} + \frac{\rho}{\mu}\big(1 - e^{-\mu t}\big).$$

Hence for all $t \geq 0$,

$$0 \leq N(t) \leq \max\{N(0), \rho/\mu\} \leq \rho/\mu + N(0),$$

and in particular $N(t) \leq \rho/\mu$ for all $t \geq 0$ provided $N(0) \leq \rho/\mu$. Thus Ω is bounded in the N-component. We will show below that Ω is positively invariant.
(ii) Positivity by boundary argument. We prove componentwise that no variable can become negative. Suppose, for the sake of contradiction, that there exists an earliest time $t^* > 0$ and an index corresponding to a state variable $X \in \{S, V, E, I_a, I_s, Q, R\}$ such that $X(t^*) = 0$ and $X(t) \geq 0$ for all $t \in [0, t^*)$ with at least one component positive on $[0, t^*)$. By continuity, all state variables satisfy $Y(t^*) \geq 0$.

We evaluate $\dot{X}(t^*)$ using the model equations and show $\dot{X}(t^*) \geq 0$, which contradicts the minimality of t^* because a negative derivative at t^* would force X to become negative immediately after t^*.

We check each state:

(a) Susceptibles S. If $S(t^*) = 0$ then from the S-equation

$$\dot{S}(t^*) = \rho - \big[\beta_s(1 - \psi\xi)I_s(t^*) + \beta_a(1 - \psi\xi)I_a(t^*)\big]S(t^*) - (\mu + \nu)S(t^*).$$

Since $S(t^*) = 0$ the infection and removal terms vanish, hence $\dot{S}(t^*) = \rho \geq 0$; therefore S cannot cross to negative values.

(b) Vaccinated V. If $V(t^*) = 0$ then from the V-equation

$$\dot{V}(t^*) = \nu S(t^*) + \gamma R(t^*) - (1 - \epsilon)\omega\big[\beta_s(1 - \psi\xi)I_s(t^*) + \beta_a(1 - \psi\xi)I_a(t^*)\big]V(t^*) - \mu V(t^*).$$

All terms proportional to $V(t^*)$ vanish. By the minimality of t^* we have $S(t^*) \geq 0$ and $R(t^*) \geq 0$, thus the remaining terms are nonnegative and consequently $\dot{V}(t^*) \geq 0$. In particular, if $\nu S(t^*) + \gamma R(t^*) > 0$ then $\dot{V}(t^*) > 0$ (so V immediately becomes positive); if $\nu S(t^*) + \gamma R(t^*) = 0$ then $\dot{V}(t^*) = 0$ and V remains at zero locally, but not negative. Either way $\dot{V}(t^*) < 0$ is impossible.

(c) Exposed E. If $E(t^*) = 0$ then

$$\dot{E}(t^*) = [\beta_s(1 - \psi\xi)I_s(t^*) + \beta_a(1 - \psi\xi)I_a(t^*)]\big(S(t^*) + (1 - \epsilon)\omega V(t^*)\big) - (\mu + \varphi)E(t^*).$$

The last term vanishes and the prefactors are nonnegative by the induction hypothesis, so $\dot{E}(t^*) \geq 0$.

(d) Infectious classes I_a, I_s. If $I_a(t^*) = 0$ then

$$\dot{I}_a(t^*) = \theta\varphi E(t^*) - (\alpha_a + \mu)I_a(t^*) = \theta\varphi E(t^*) \geq 0,$$

and similarly for I_s with $(1 - \theta)\varphi E(t^*) \geq 0$.

(e) Quarantined Q**.** If $Q(t^*) = 0$ then

$$\dot{Q}(t^*) = \eta\alpha_a I_a(t^*) + \sigma\alpha_s I_s(t^*) - (\lambda_q + \mu)Q(t^*) = \eta\alpha_a I_a(t^*) + \sigma\alpha_s I_s(t^*) \geq 0.$$

(f) Recovered R**.** If $R(t^*) = 0$ then

$$\dot{R}(t^*) = (1-\eta)\alpha_a I_a(t^*) + (1-\sigma)\alpha_s I_s(t^*) + \lambda_q Q(t^*) - (\mu + \gamma)R(t^*),$$

and the right-hand side is nonnegative because all source terms are nonnegative and $R(t^*) = 0$ annuls the loss term. Hence $\dot{R}(t^*) \geq 0$.

In every case we obtain $\dot{X}(t^*) \geq 0$, which contradicts the assumption that X becomes negative immediately after t^*. Therefore no component can become negative at any finite time; i.e. the nonnegative orthant is forward invariant and all state variables remain nonnegative for all $t \geq 0$.

(iii) Positive invariance of Ω. From part (i) we have $N(t) \leq \rho/\mu$ for all $t \geq 0$ (when $N(0) \leq \rho/\mu$), and from part (ii) all components are nonnegative. Hence the trajectory starting in Ω never leaves Ω, so Ω is positively invariant.

This completes the proof. □

Theorem 2.2. *The feasible region* Ω *defined in* (2.4) *is positively invariant and bounded in* $\mathbb{R}^7_+$*. In particular, the total population* $N(t)$ *satisfies*

$$0 \leq N(t) \leq \frac{\rho}{\mu}, \qquad \forall t \geq 0.$$

Proof. By summing all the equations of system (2.2), we obtain

$$\frac{dN}{dt} = \rho - \mu N.$$

This linear ODE can be solved explicitly. Separating variables and integrating gives

$$\int \frac{dN}{\rho - \mu N} = \int dt \quad \Rightarrow \quad -\frac{1}{\mu}\ln(\rho - \mu N) = t + c,$$

where c is the constant of integration. Rearranging,

$$\rho - \mu N = Ae^{-\mu t}, \qquad A > 0.$$

Thus,

$$N(t) = \frac{\rho}{\mu} - \frac{A}{\mu}e^{-\mu t}. \tag{2.5}$$

Imposing the initial condition $N(0) = N_0$ gives

$$A = \rho - \mu N_0,$$

so that

$$N(t) = \frac{\rho}{\mu} - \Big(\frac{\rho - \mu N_0}{\mu}\Big)e^{-\mu t}. \tag{2.6}$$

From (2.6) it is clear that $N(t)$ is nonnegative for all $t \geq 0$ provided $N_0 \geq 0$, and moreover

$$\lim_{t\to\infty} N(t) = \frac{\rho}{\mu}.$$

Since $e^{-\mu t} \geq 0$ for all t, we also have

$$0 \leq N(t) \leq \frac{\rho}{\mu}, \qquad \forall t \geq 0.$$

Therefore the feasible region $\Omega = \{(S, V, E, I_a, I_s, Q, R) \in \mathbb{R}^7_+ : N(t) \leq \rho/\mu\}$ is positively invariant and bounded. □

3. Mathematical analysis of the model

3.1. **The disease-free equilibrium point of the model.** To obtain the equilibrium points, we put the right-hand side of model (2.2) equal to zero and get

$$\begin{aligned}
\rho - [\beta_s(1-\psi\xi)I_s + \beta_a(1-\psi\xi)I_a]S - (\mu+\nu)S = 0,\\
\nu S + \gamma R - (1-\epsilon)\omega[\beta_s(1-\psi\xi)I_s + \beta_a(1-\psi\xi)I_a]V - \mu V = 0,\\
[\beta_s(1-\psi\xi)I_s + \beta_a(1-\psi\xi)I_a](S + (1-\epsilon)\omega V) - (\mu+\varphi)E = 0,\\
\theta\varphi E - (\alpha_a+\mu)I_a = 0,\\
(1-\theta)\varphi E - (\alpha_s+\mu)I_s = 0,\\
\eta\alpha_a I_a + \sigma\alpha_s I_s - (\lambda_q+\mu)Q = 0,\\
(1-\eta)\alpha_a I_a + (1-\sigma)\alpha_s I_s + \lambda_q Q - (\mu+\gamma)R = 0.
\end{aligned} \tag{3.1}$$

We denote the disease-free equilibrium point ($DFEP$) as

$$\mathbf{X}_{dfep} = (S_{dfep}, V_{dfep}, E_{dfep}, I_{a\ dfep}, I_{s\ dfep}, Q_{dfep}, R_{dfep}).$$

We have $DFEP$ when COVID-19 is absent in the population. Thus if we put $E = I_a = I_s = Q = R = 0$ in the system (3.1), then $DFEP$ of the model (2.2) will be as follows:

$$\mathbf{X}_{dfep} = (\frac{\rho}{\mu+\nu}, \frac{\rho\nu}{\mu(\mu+\nu)}, 0, 0, 0, 0, 0),$$

3.2. **The basic reproduction number of model (2.2).** The model basic reproduction number is shown by $\mathcal{R}_0$, which determines the spread or otherwise of the infection into the entire population. We follow the next-generation matrix method, which was described by van den Driessche and Watmough [**?**]. The compartments that directly cause the spread of COVID-19 are from the third, fourth, and fifth equations of the model (2.2). So

$$\begin{aligned}
\frac{dE}{dt} &= [\beta_s(1-\psi\xi)I_s + \beta_a(1-\psi\xi)I_a](S + (1-\epsilon)\omega V) - (\mu+\varphi)E,\\
\frac{dI_a}{dt} &= \theta\varphi E - (\alpha_a+\mu)I_a,\\
\frac{dI_s}{dt} &= (1-\theta)\varphi E - (\alpha_s+\mu)I_s.
\end{aligned} \tag{3.2}$$

We can write the system (3.2) as $\frac{dy}{dt} = \Phi(y) - \Psi(y)$, where

$$y = (E, I_a, I_s)^T, \qquad \Psi(y) = \begin{bmatrix} (\mu+\varphi)E \\ -\theta\varphi E + (\mu+\alpha_a)I_a \\ -(1-\theta)\varphi E + (\mu+\alpha_s)I_s \end{bmatrix},$$

and

$$\Phi(y) = \begin{bmatrix} [\beta_s(1-\psi\xi)I_s + \beta_a(1-\psi\xi)I_a](S + (1-\epsilon)\omega V) \\ 0 \\ 0 \end{bmatrix}.$$

We define F and V the Jacobian matrices of Φ and Ψ at the $DFEP(\mathbf{X}_{dfep})$, respectively, which are given by

$$F = J(\Phi|\mathbf{X}_{dfep}) = \begin{bmatrix} 0 & \frac{\beta_a(1-\psi\xi)\rho(\mu+(1-\epsilon)\omega\nu)}{\mu(\mu+\nu)} & \frac{\beta_s(1-\psi\xi)\rho(\mu+(1-\epsilon)\omega\nu)}{\mu(\mu+\nu)} \\ 0 & 0 & 0 \\ 0 & 0 & 0 \end{bmatrix},$$

$$V = J(\Psi|\mathbf{X}_{dfep}) = \begin{bmatrix} \mu+\varphi & 0 & 0 \\ -\theta\varphi & \mu+\alpha_a & 0 \\ -(1-\theta)\varphi & 0 & \mu+\alpha_s \end{bmatrix}.$$

We obtain FV^{-1} as the following form:

$$FV^{-1} = \begin{bmatrix} \frac{\beta_a(1-\psi\xi)\rho(\mu+(1-\epsilon)\omega\nu)\theta\varphi}{\mu(\mu+\nu)(\mu+\varphi)(\mu+\alpha_a)} + \frac{\beta_s(1-\psi\xi)\rho(\mu+(1-\epsilon)\omega\nu)(1-\theta)\varphi}{\mu(\mu+\nu)(\mu+\varphi)(\mu+\alpha_s)} & \frac{\beta_a(1-\psi\xi)\rho(\mu+(1-\epsilon)\omega\nu)}{\mu(\mu+\nu)(\mu+\alpha_a)} & \frac{\beta_s(1-\psi\xi)\rho(\mu+(1-\epsilon)\omega\nu)}{\mu(\mu+\nu)(\mu+\alpha_s)} \\ 0 & 0 & 0 \\ 0 & 0 & 0 \end{bmatrix}.$$

Two eigenvalues of the above matrix are zero, and the third eigenvalue is equal to

$$\frac{\beta_a(1-\psi\xi)\rho(\mu+(1-\epsilon)\omega\nu)\theta\varphi}{\mu(\mu+\nu)(\mu+\varphi)(\mu+\alpha_a)} + \frac{\beta_s(1-\psi\xi)\rho(\mu+(1-\epsilon)\omega\nu)(1-\theta)\varphi}{\mu(\mu+\nu)(\mu+\varphi)(\mu+\alpha_s)}.$$

Moreover, $\mathcal{R}_0$ will be the largest eigenvalue (the spectral radius) of the matrix FV^{-1}. Thus the basic reproduction number is given by

$$\mathcal{R}_0 = \frac{\beta_a(1-\psi\xi)\rho(\mu+(1-\epsilon)\omega\nu)\theta\varphi}{\mu(\mu+\nu)(\mu+\varphi)(\mu+\alpha_a)} + \frac{\beta_s(1-\psi\xi)\rho(\mu+(1-\epsilon)\omega\nu)(1-\theta)\varphi}{\mu(\mu+\nu)(\mu+\varphi)(\mu+\alpha_s)}. \tag{3.3}$$

The basic reproduction number $\mathcal{R}_0$ implies the average number of secondary infections generated by a single infectious individual during his entire duration of infectiousness in a totally susceptible population when vaccination is implemented.

3.3. **Existence of an endemic equilibrium.** The endemic equilibrium point (EEP) is denoted by

$$\mathbf{X}_{eep} = (S_{eep}, V_{eep}, E_{eep}, I_{a\ eep}, I_{s\ eep}, Q_{eep}, R_{eep}),$$

where

$$\begin{aligned}
S_{eep} &= \frac{\rho}{\beta_s(1-\psi\xi)I_s + \beta_a(1-\psi\xi)I_a + \mu + \nu}, \\
V_{eep} &= \frac{\nu S + \gamma R}{(1-\epsilon)\omega[\beta_s(1-\psi\xi)I_s + \beta_a(1-\psi\xi)I_a] + \mu}, \\
E_{eep} &= \frac{(S + (1-\epsilon)\omega V)[\beta_s(1-\psi\xi)I_s + \beta_a(1-\psi\xi)I_a]}{\mu+\varphi}, \\
I_{a\ eep} &= \frac{\theta\varphi E}{\mu+\alpha_a}, \\
I_{s\ eep} &= \frac{(1-\theta)\varphi E}{\mu+\alpha_s}, \\
Q_{eep} &= \frac{\eta\alpha_a I_a + \sigma\alpha_s I_s}{\mu+\lambda_q}, \\
R_{eep} &= \frac{(1-\eta)\alpha_a I_a + (1-\sigma)\alpha_s I_s + \lambda_q}{\mu+\gamma}.
\end{aligned} \tag{3.4}$$

We now prove rigorously that an endemic equilibrium (EEP) with $(E_{eep}, I_{a\ eep}, I_{s\ eep}) \neq (0,0,0)$ exists if the basic reproduction number $\mathcal{R}_0$ exceeds unity.

In the following, we provide a rigorous proof of the existence of an endemic equilibrium using $G'(0)$.

Notation. Define the force of infection

$$\Lambda := (1-\psi\xi)(\beta_s I_s + \beta_a I_a).$$

From the equilibrium relations in (3.1) we set

$$c_a = \frac{\theta\varphi}{\mu+\alpha_a}, \qquad c_s = \frac{(1-\theta)\varphi}{\mu+\alpha_s},$$

so that $I_a = c_a E,\ I_s = c_s E$. Define

$$K := (1-\psi\xi)(\beta_a c_a + \beta_s c_s) > 0.$$

Using the third equilibrium equation of (3.1),

$$(\mu+\varphi)E = (S+(1-\epsilon)\omega V)\Lambda,$$

hence

$$E = A(S,V)\Lambda, \qquad A(S,V) := \frac{S+(1-\epsilon)\omega V}{\mu+\varphi} \geq 0.$$

Combining with $\Lambda = KE$ gives the self-consistency relation

$$\Lambda = K\,A(S(\Lambda),V(\Lambda))\,\Lambda.$$

Nontrivial equilibria $\Lambda > 0$ exist precisely when

$$F(\Lambda) := K\,A(S(\Lambda),V(\Lambda)) - 1 = 0.$$

At $\Lambda = 0$,

$$F(0) = \mathcal{R}_0 - 1,$$

where $\mathcal{R}_0 = K\,A(S(0),V(0))$ is the basic reproduction number evaluated at the DFEP.

Existence. The function $F : [0,\infty) \to \mathbb{R}$ is continuous. Moreover $S(\Lambda), V(\Lambda) \to 0$ as $\Lambda \to \infty$, so $A(S,V) \to 0$ and $F(\Lambda) \to -1 < 0$. Thus if $\mathcal{R}_0 > 1$ we have $F(0) > 0$ and by the intermediate value theorem there exists $\Lambda^* > 0$ with $F(\Lambda^*) = 0$. Substitution yields a strictly positive endemic equilibrium $\mathbf{X}_{eep}$.

Derivative at zero. Differentiating gives

$$F'(\Lambda) = \frac{K}{\mu+\varphi}\Big(S'(\Lambda) + (1-\epsilon)\omega V'(\Lambda)\Big).$$

A short calculation yields

$$S'(0) = -\frac{\rho}{(\mu+\nu)^2}, \qquad V'(0) = -\frac{\nu\rho\big(\mu+(1-\epsilon)\omega(\mu+\nu)\big)}{\mu^2(\mu+\nu)^2},$$

so

$$F'(0) < 0.$$

Thus

$$\mathcal{R}_0 > 1 \quad \Longrightarrow \quad F(0) > 0 \text{ and } F'(0) < 0,$$

ensuring the existence of a positive root.

4. Stability analysis

4.1. Local stability of the DFEP.

Theorem 4.1. *The DFEP($\mathbf{X}_{dfep}$) is locally asymptotically stable if $\mathcal{R}_0 < 1$, and it is unstable if $\mathcal{R}_0 > 1$.*

Proof. In this proof, the following conventions are used:

$$a_1 = \mu+\nu, \qquad a_2 = \mu+\varphi, \qquad a_3 = \mu+\alpha_a,$$
$$a_4 = \mu+\alpha_s, \qquad a_5 = \mu+\lambda_q, \qquad a_6 = \mu+\gamma,$$
$$k_1 = \frac{\rho(1-\psi\xi)}{\mu+\nu}, \qquad k_2 = \frac{(1-\epsilon)\omega(1-\psi\xi)\rho\nu}{\mu(\mu+\nu)}, \qquad k_3 = k_1+k_2.$$

The Jacobian matrix of (2.2) at the $DFEP$ is given by

$$J(\mathbf{X}_{dfep}) = \begin{bmatrix} -a_1 & 0 & 0 & -k_1\beta_a & -k_1\beta_s & 0 & 0 \\ \nu & -\mu & 0 & -k_2\beta_a & -k_2\beta_s & 0 & \gamma \\ 0 & 0 & -a_2 & k_3\beta_a & k_3\beta_s & 0 & 0 \\ 0 & 0 & \theta\varphi & -a_3 & 0 & 0 & 0 \\ 0 & 0 & (1-\theta)\varphi & 0 & -a_4 & 0 & 0 \\ 0 & 0 & 0 & \eta\alpha_a & \sigma\alpha_s & -a_5 & 0 \\ 0 & 0 & 0 & (1-\eta)\alpha_a & (1-\sigma)\alpha_s & \lambda_q & -a_6 \end{bmatrix}.$$

The characteristic polynomial equation for the above matrix has the following form:

$$(\lambda+\mu)(\lambda+a_1)(\lambda+a_5)(\lambda+a_6)(\lambda^3+\lambda^2 m_1+\lambda m_2+m_3)=0,$$

where

$$\begin{aligned} m_1 &= a_2+a_3+a_4, \\ m_2 &= a_2a_4+a_3a_4+a_2a_3-k_3\beta_a\theta\varphi-k_3\beta_s(1-\theta)\varphi, \\ m_3 &= a_2a_3a_4-k_3\beta_a\theta\varphi a_4-k_3\beta_s(1-\theta)\varphi a_3. \end{aligned}$$

Here, four eigenvalues have a negative real part. According to Routh–Hurwitz criteria, a sufficient condition for the roots of polynomial $\lambda^3+\lambda^2 m_1+\lambda m_2+m_3$ to be negative or have a negative real part is that $m_1, m_2, m_3 > 0$ and $m_1 m_2 > m_3$.

In order to check these conditions of the Routh–Hurwitz criteria, we rewrite the coefficients m_1, m_2, and m_3 in terms of the basic reproduction number given by (3.3):

$$\begin{aligned} m_1 &= a_2+a_3+a_4, \\ m_2 &= (1-\mathcal{R}_0)(a_2a_4+a_3a_4+a_2a_3)+\beta_a k_3\theta\varphi a_4\Big(\frac{1}{a_2}+\frac{1}{a_3}\Big)+\beta_s k_3(1-\theta)\varphi a_3\Big(\frac{1}{a_2}+\frac{1}{a_4}\Big), \\ m_3 &= a_2a_3a_4(1-\mathcal{R}_0). \end{aligned}$$

Also, we compute, in terms of $\mathcal{R}_0$, the following expression:

$$\begin{aligned} m_1m_2-m_3 &= (1-\mathcal{R}_0)(a_2^2a_4+a_2^2a_3) \\ &\quad +(1-\mathcal{R}_0)(a_2a_4+a_3a_4+a_2a_3)(a_3+a_4) \\ &\quad +(a_2+a_3+a_4)[\beta_a k_3\theta\varphi a_4\Big(\frac{1}{a_2}+\frac{1}{a_3}\Big)+\beta_s k_3(1-\theta)\varphi a_3\Big(\frac{1}{a_2}+\frac{1}{a_4}\Big)]. \end{aligned}$$

It is clear that if $\mathcal{R}_0 < 1$, then the conditions of Routh–Hurwitz are satisfied, and as a result, the $DFEP$ is stable. In the case when $\mathcal{R}_0 > 1$, we have $m_3 < 0$ and by using Descartes' rule of signs, we conclude that at least one of the eigenvalues is positive. As a consequence, the system will be unstable. □

4.2. **Global stability of the DFEP.** In this section, we prove that the $DFEP$ has globally stability. We do this via a scalar function, which is called the Lyapunov function.

Theorem 4.2. *The $DFEP$ of model (2.2) is globally asymptotically stable if $\mathcal{R}_0 < 1$.*

Proof. We first construct the Lyapunov function, and then we show that its time derivative is globally negative. Let

$$\mathcal{L}_{DFEP} = B_1E + B_2I_a + B_3I_s, \tag{4.1}$$

where

$$\begin{aligned} B_1 &= (\mu+\alpha_a)(\mu+\alpha_s), \\ B_2 &= (\mu+\alpha_s)\beta_a(1-\psi\xi)\Big(\frac{\rho}{\mu+\nu}+(1-\epsilon)\omega\frac{\rho\nu}{\mu(\mu+\nu)}\Big), \end{aligned}$$

$$B_3 = (\mu+\alpha_a)\beta_s(1-\psi\xi)\Big(\frac{\rho}{\mu+\nu} + (1-\epsilon)\omega\frac{\rho\nu}{\mu(\mu+\nu)}\Big). \tag{4.2}$$

Then the derivation of function (4.1) is

$$\frac{\partial \mathcal{L}_{DFEP}}{\partial t} = B_1\frac{dE}{dt} + B_2\frac{dI_a}{dt} + B_3\frac{dI_s}{dt}.$$

By substituting equal values from model (2.2) instead of $\frac{dE}{dt}$, $\frac{dI_a}{dt}$, and $\frac{dI_s}{dt}$ at the $DFEP$, we have

$$\begin{aligned}\frac{\partial \mathcal{L}_{DFEP}}{\partial t} &= B_1([\beta_s(1-\psi\xi)I_s + \beta_a(1-\psi\xi)I_a]\Big(\frac{\rho}{\mu+\nu} + (1-\epsilon)\omega\frac{\rho\nu}{\mu(\mu+\nu)}) - (\mu+\varphi)E\Big)\\ &+ B_2[\theta\varphi E - (\alpha_a+\mu)I_a]\\ &+ B_3[(1-\theta)\varphi E - (\alpha_s+\mu)I_s].\end{aligned} \tag{4.3}$$

The expansion of (4.3) yields

$$\begin{aligned}\frac{\partial \mathcal{L}_{DFEP}}{\partial t} &= (\mu+\alpha_a)(\mu+\alpha_s)([\beta_s(1-\psi\xi)I_s + \beta_a(1-\psi\xi)I_a] \times \Big(\frac{\rho}{\mu+\nu} + (1-\epsilon)\omega\frac{\rho\nu}{\mu(\mu+\nu)}) - (\mu+\varphi)E\Big)\\ &+ (\mu+\alpha_s)\beta_a(1-\psi\xi)\Big(\frac{\rho}{\mu+\nu} + (1-\epsilon)\omega\frac{\rho\nu}{\mu(\mu+\nu)}\Big)[\theta\varphi E - (\alpha_a+\mu)I_a]\\ &+ (\mu+\alpha_a)\beta_s(1-\psi\xi)\Big(\frac{\rho}{\mu+\nu} + (1-\epsilon)\omega\frac{\rho\nu}{\mu(\mu+\nu)}\Big)[(1-\theta)\varphi E - (\alpha_s+\mu)I_s].\end{aligned} \tag{4.4}$$

Then (4.4) becomes

$$\begin{aligned}\frac{\partial \mathcal{L}_{DFEP}}{\partial t} &= (\mu+\alpha_s)(\mu+\alpha_a)[\beta_a(1-\psi\xi)I_a]\Big(\frac{\rho}{\mu+\nu} + (1-\epsilon)\omega\frac{\rho\nu}{\mu(\mu+\nu)}\Big)\\ &- (\mu+\alpha_s)(\mu+\alpha_a)[\beta_a(1-\psi\xi)I_a]\Big(\frac{\rho}{\mu+\nu} + (1-\epsilon)\omega\frac{\rho\nu}{\mu(\mu+\nu)}\Big)\\ &+ (\mu+\alpha_a)(\mu+\alpha_s)[\beta_s(1-\psi\xi)I_s]\Big(\frac{\rho}{\mu+\nu} + (1-\epsilon)\omega\frac{\rho\nu}{\mu(\mu+\nu)}\Big)\\ &- (\mu+\alpha_a)(\mu+\alpha_s)[\beta_s(1-\psi\xi)I_s]\Big(\frac{\rho}{\mu+\nu} + (1-\epsilon)\omega\frac{\rho\nu}{\mu(\mu+\nu)}\Big)\\ &+ (\mu+\alpha_s)\beta_a(1-\psi\xi)\Big(\frac{\rho}{\mu+\nu} + (1-\epsilon)\omega\frac{\rho\nu}{\mu(\mu+\nu)}\Big)\theta\varphi E\\ &+ (\mu+\alpha_a)\beta_s(1-\psi\xi)\Big(\frac{\rho}{\mu+\nu} + (1-\epsilon)\omega\frac{\rho\nu}{\mu(\mu+\nu)}\Big)(1-\theta)\varphi E\\ &- (\mu+\alpha_a)(\mu+\alpha_s)(\mu+\varphi)E.\end{aligned} \tag{4.5}$$

The sum of the first four terms on the right-hand side of the (4.5) is zero. Thus,

$$\begin{aligned}\frac{\partial \mathcal{L}_{DFEP}}{\partial t} &= (\mu+\alpha_s)\beta_a(1-\psi\xi)\Big(\frac{\rho}{\mu+\nu} + (1-\epsilon)\omega\frac{\rho\nu}{\mu(\mu+\nu)}\Big)\theta\varphi E\\ &+ (\mu+\alpha_a)\beta_s(1-\psi\xi)\Big(\frac{\rho}{\mu+\nu} + (1-\epsilon)\omega\frac{\rho\nu}{\mu(\mu+\nu)}\Big)(1-\theta)\varphi E\\ &- (\mu+\alpha_a)(\mu+\alpha_s)(\mu+\varphi)E.\end{aligned}$$

Therefore,

$$\begin{aligned}\frac{\partial \mathcal{L}_{DFEP}}{\partial t} &= (\mu+\alpha_a)(\mu+\alpha_s)(\mu+\varphi) \times \left[\frac{\beta_a(1-\psi\xi)(\mu+(1-\epsilon)\omega\nu)\rho\theta\varphi}{\mu(\mu+\nu)(\mu+\varphi)(\mu+\alpha_a)} + \frac{\beta_s(1-\psi\xi)(\mu+(1-\epsilon)\omega\nu)\rho(1-\theta)\varphi}{\mu(\mu+\nu)(\mu+\varphi)(\mu+\alpha_s)} - 1\right]E\\ &= (\mu+\alpha_a)(\mu+\alpha_s)(\mu+\varphi)[\mathcal{R}_0 - 1]E.\end{aligned}$$

Since all parameters are assumed to be positive and according to Theorem 2.1, the variable E is positive, thus $\frac{\partial \mathcal{L}_{DFEP}}{\partial t} \leq 0$. □

4.3. **Local stability of the EEP.**

Lemma 4.3. *The endemic equilibrium point* $\mathbf{X}_{eep}$ *of the model* (2.2) *exists with strictly positive infective components if* $\mathcal{R}_0 > 1$.

Proof. See the detailed existence proof in Section 3.3, where the self-consistency relation for the force of infection Λ is derived and a positive root $\Lambda^* > 0$ is guaranteed by the intermediate value theorem. Substituting Λ^* into the algebraic relations yields positive values for E, I_a, I_s, Q, R, S, V, and thus $\mathbf{X}_{eep}$ exists with all components positive. □

Theorem 4.4. *If* $\mathcal{R}_0 > 1$, *the endemic equilibrium* $\mathbf{X}_{eep}$ *is locally asymptotically stable in* Ω.

Proof. The local stability of $\mathbf{X}_{eep}$ can be established by linearizing the system (2.2) at $\mathbf{X}_{eep}$ and checking the eigenvalues of the Jacobian matrix. Standard results for SEIR-type models with vaccination and quarantine compartments imply that if $\mathcal{R}_0 > 1$, all eigenvalues of the Jacobian have negative real parts, except possibly one associated with a zero eigenvalue corresponding to conservation of total population. Thus, $\mathbf{X}_{eep}$ is locally asymptotically stable. □

Remark 4.5. The global asymptotic stability of the endemic equilibrium in the full seven-dimensional system is nontrivial. While the divergence calculation may suggest dissipative behavior, a rigorous proof would require advanced methods such as Li–Muldowney's geometric approach or construction of a suitable Lyapunov function. In this study, we establish only local asymptotic stability.

Remark 4.6. To avoid any ambiguity regarding the sources of data and parameter values, in this study we explicitly made the following distinction. The data used for model fitting such as the monthly reported cases and the sequence of epidemic waves were obtained from published studies and reliable databases, including the Johns Hopkins University Coronavirus Resource Center. On the other hand, for certain clinical and behavioral parameters for which reliable local estimates from Iran were not available (for example, the infectious period, the transition rates from classes (I_a) and (I_s), or some empirical values related to recovery rates under quarantine), we adopted parameter values reported in the international literature (for instance, the study from Bangkok cited in Table **??**). The rationale for this choice is that such studies provide direct biological and clinical estimates that are generally transferable across urban populations. To ensure transparency, we have added a column in Table **??** to clearly indicate the origin of each parameter. Furthermore, to demonstrate the robustness of our results with respect to uncertainty in these borrowed parameters, we performed a sensitivity analysis (Section 7) over plausible parameter ranges. The results confirm that the overall outcomes and the main messages of the study remain stable under reasonable variations of these parameters. In addition, it is important to note that the model itself is not directly used to estimate each parameter value. Rather, the model fitting focuses on reproducing the overall epidemic dynamics such as the timing and relative magnitude of successive waves by using the available data and adjusting a limited subset of parameters (mainly transmission-related coefficients) within biologically reasonable ranges. The remaining parameters were fixed according to clinical or published sources. This approach ensures that the fitted model reflects realistic epidemic behavior while maintaining scientific transparency.

5. Data Fitting

In this section, we analyze the monthly confirmed COVID-19 cases in Iran from March 31, 2020, to July 31, 2021 [**?**]. The aim of this analysis is to qualitatively compare the observed epidemic pattern with the temporal dynamics predicted by our compartmental model. To obtain a descriptive representation of the empirical epidemic trajectory, we employed a simple polynomial curve to approximate the monthly reported cases during each wave. This descriptive fitting serves as a reference to examine whether the overall behavior of the observed data such as the accelerating rise, the peak, and the subsequent decline is consistent with the qualitative features theoretically generated by our model under comparable parameter regimes (see Table **??**). The fitted polynomial captures the main trends observed in each epidemic wave, including the early exponential-like growth and the later stabilization phase, both of which are in agreement with the model's theoretical predictions. The quality of the descriptive fitting was evaluated using statistical indicators such as the root mean squared error (RMSE) and the coefficient of determination (R^2). The results for the four epidemic waves are shown in Figures 2-6, demonstrating a good overall agreement between the reported data and

TABLE 2. COVID-19 total confirmed cases for the first wave in Iran.

Months	Total Confirmed Cases
March 31, 2020	44,605
April 30, 2020	94,640
May 31, 2020	151,466
June 30, 2020	227,662

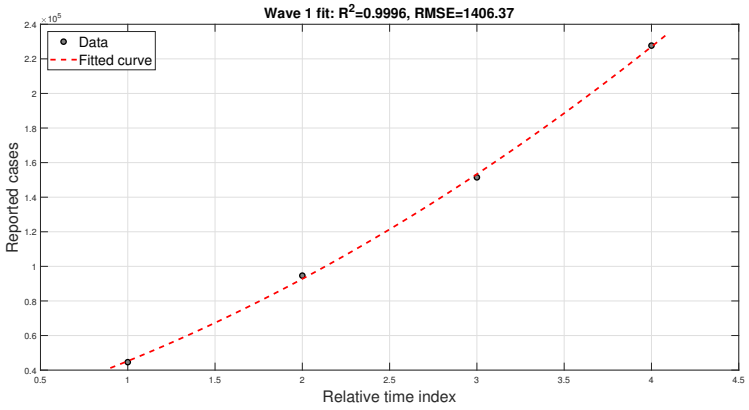

FIGURE 2. The observed monthly cumulative cases (for Iran) are approximated by a quadratic polynomial, from March 31, 2020 to June 30, 2020 (first wave).

the polynomial representation of the epidemic evolution in Iran. By July 31, 2021, Iran had experienced four major COVID-19 waves [**?**]. The corresponding time spans and total monthly confirmed cases are listed in Tables 2-5. The polynomial curves shown in Figures 2-6 are therefore used as descriptive approximations to visualize the data and to facilitate a qualitative comparison with the behavior predicted by model (2.2). Figure 2 presents the fitting of the first wave of COVID-19 in Iran (March-June 2020) using a quadratic polynomial model. The black circles denote the reported cumulative cases over four consecutive months, while the red dashed line represents the fitted curve. The estimated quadratic function is expressed as:

$$C(t) = a_2 t^2 + a_1 t + a_0, \tag{5.1}$$

with the fitted coefficients:

$$a_2 = 6.540250 \times 10^3, \quad a_1 = 2.789845 \times 10^4, \quad a_0 = 1.079525 \times 10^4.$$

The fitted quadratic function captures the accelerating growth trend observed during the first wave. The high coefficient of determination ($R^2 = 0.9996$) indicates that the model explains nearly all the variability in the data. The root mean squared error (RMSE = 1,406.37) is relatively small compared to the scale of the data, suggesting that prediction errors are negligible in practical terms. From an epidemiological perspective, the fitted curve highlights the rapid escalation of reported cases during the early stage of the epidemic. The upward curvature of the polynomial reflects the accelerating growth pattern typically observed when effective interventions (e.g., lockdowns or social distancing) are not immediately implemented. These results underscore the importance of timely public health measures to prevent further surges of infection. Figure 3 illustrates the growth of the total confirmed COVID-19 cases during the second wave in Iran, covering the period from July 31 to October 31, 2020. The black circles represent the actual reported data at four time points (304,204 on July 31; 375,212 on August 31; 457,219 on September 30; and 612,772 on October 31). The fitted curve (blue dashed line) captures the trend of the epidemic wave using a quadratic polynomial model.

TABLE 3. COVID-19 total confirmed cases for second wave in Iran.

Months	Total confirmed cases		
July 31, 2020	304204	August 31, 2020	375212
Sep 30, 2020	457219	Oct 31, 2020	612772

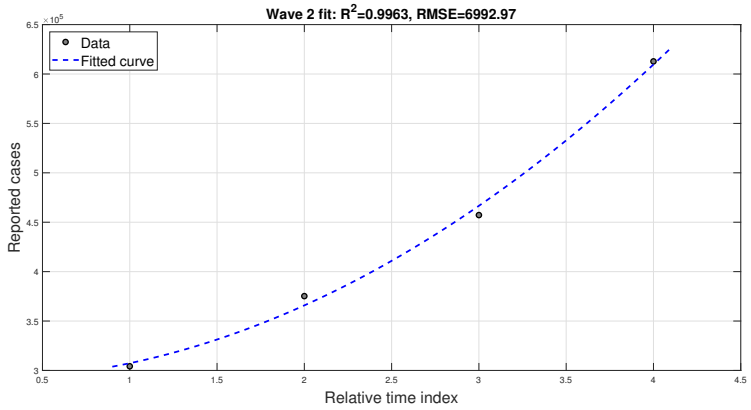

FIGURE 3. The observed monthly cumulative cases (for Iran) are approximated by a quadratic polynomial, from July 31, 2020 to October 31, 2020 (second wave).

TABLE 4. COVID-19 total confirmed cases for third wave in Iran.

Months	Total confirmed cases	Months	Total confirmed cases
Nov 30, 2020	962070	Feb 28, 2021	1631169
Dec 31, 2020	1225142	March 31, 2021	1885564
Jan 31, 2021	1417999		

The fitted quadratic model describing the cumulative cases is expressed as:

$$C(t) = a_2 t^2 + a_1 t + a_0, \tag{5.2}$$

with the parameter values determined as

$$a_2 = 2.113625 \times 10^4, \quad a_1 = -4.910150 \times 10^3, \quad a_0 = 2.911053 \times 10^5.$$

The model demonstrates an excellent fit with the observed data, as reflected by the high coefficient of determination ($R^2 = 0.9963$). The root mean square error (RMSE = 6992.97) is negligible compared to the magnitude of the reported cases (hundreds of thousands), confirming the robustness and reliability of the fitting process.

From an epidemiological perspective, the results clearly reveal a rapid, nonlinear (quasi-exponential) increase in the total number of cases, with the cumulative count approximately doubling within three months. This trend highlights the high transmission intensity of COVID-19 during the second wave in Iran and demonstrates the potential of the fitted polynomial model to provide accurate projections for future epidemic dynamics and associated healthcare burdens.

Figure 4 presents the progression of total confirmed COVID-19 cases in Iran during the third wave, spanning the period from November 30, 2020, to March 31, 2021. The black circles denote the observed data points, including 962,070 cases on November 30, 1,225,142 cases on December 31, 1,417,999 cases on January 31, 1,631,169 cases on February 28, and 1,885,564 cases on March 31. The magenta dashed curve represents the fitted model, which aligns closely with the reported data.

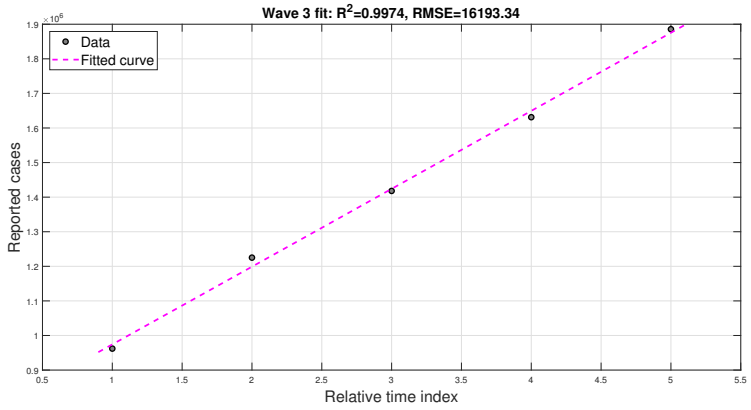

FIGURE 4. The observed monthly cumulative cases (for Iran) are approximated by a quadratic polynomial, from November 30, 2020 to March 31, 2021 (third wave).

TABLE 5. COVID-19 total confirmed cases for fourth wave in Iran.

Months	Total confirmed cases
April 30, 2021	2499077
May 31, 2021	2913136
June 30, 2021	3204557
July 31, 2021	3871008

A quadratic function was used to model the reported cumulative cases, resulting in the following expression:

$$C(t) = a_2 t^2 + a_1 t + a_0, \tag{5.3}$$

where the estimated coefficients are:

$$a_2 = 2.113571 \times 10^2, \quad a_1 = 2.240334 \times 10^5, \quad a_0 = 7.499638 \times 10^5.$$

The coefficient of determination ($R^2 = 0.9974$) indicates a highly accurate fit, and the root mean square error (RMSE = 16,193.34) remains small compared to the overall magnitude of reported cases, further confirming the robustness of the model.

Unlike the second wave, which exhibited quasi-exponential growth, the third wave shows a nearly linear increase in the cumulative number of cases, as reflected by the straight-line pattern of the fitted curve. This trend suggests a sustained but more stabilized transmission dynamic during this period, likely due to the combined effects of partial control measures, changes in public behavior, and possible immunity accumulation in the population. Overall, the third wave reflects a significant but slower-paced expansion of the epidemic compared to earlier waves, emphasizing the importance of continued interventions to suppress the spread of the disease. The fitted quadratic curve (green dashed line in Figure 5) captures the accelerating upward trend in the data. The cumulative case trend was fitted with a quadratic polynomial:

$$C(t) = a_2 t^2 + a_1 t + a_0, \tag{5.4}$$

featuring the coefficients:

$$a_2 = 6.309800 \times 10^4, \quad a_1 = 1.252314 \times 10^5, \quad a_0 = 2.335631 \times 10^6.$$

The coefficient of determination ($R^2 = 0.9876$) indicates that 98.76% of the data variability is explained by the model, and the root mean square error (RMSE = 55,640.97) corresponds to a relative error of less than 2%, confirming a good fit.

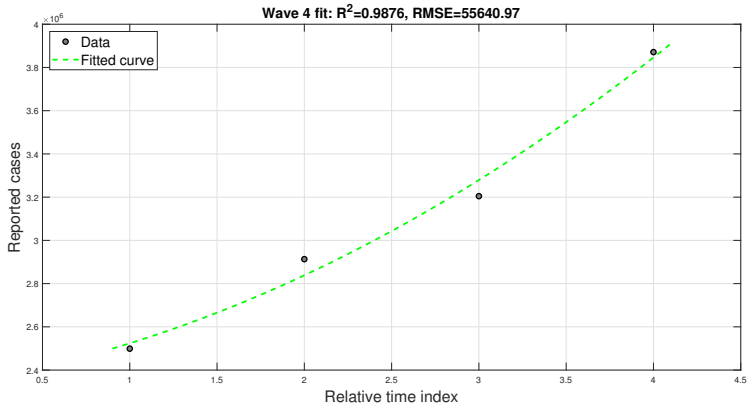

FIGURE 5. The observed monthly cumulative cases (for Iran) are approximated by a quadratic polynomial, from April 30, 2021 to July 31, 2021 (fourth wave).

From an epidemiological perspective, the sharp increase, especially between June and July, reflects a high transmission rate, suggesting that the outbreak had not yet peaked and that timely public health interventions such as accelerated vaccination campaigns or temporary social restrictions were necessary to prevent further escalation.

Figure 6 presents the overall fitting of the cumulative confirmed COVID-19 cases in Iran, covering the combined period of the first through fourth epidemic waves (March 2020-August 2021). The black circles represent the reported cumulative cases at multiple monthly time points, while the brown dashed curve indicates the fitted quadratic polynomial model.

The optimal quadratic fit for the cumulative cases is represented by:

$$C(t) = at^2 + bt + c, \tag{5.5}$$

with the corresponding parameter estimates:

$$a = 1.65282 \times 10^4, \quad b = -6.97255 \times 10^4, \quad c = 1.78982 \times 10^5.$$

The model achieved a coefficient of determination of $R^2 = 0.9957$, indicating that 99.57% of the variance in the observed cumulative cases is explained by the fitted curve. The root mean square error (RMSE = 77,284.86) is relatively small compared to the total magnitude of cases (on the order of millions), confirming that the quadratic model provides a highly accurate representation of the data.

From an epidemiological viewpoint, the upward curvature of the fitted polynomial reflects a consistent acceleration in cumulative cases across the four waves, demonstrating that despite temporal fluctuations in transmission dynamics during individual waves, the overall trend of the epidemic followed a sustained growth pattern. The initial mild increase followed by a sharp upward trend after mid-2020 suggests that although early interventions temporarily slowed transmission, subsequent relaxation of control measures and the emergence of new variants likely contributed to renewed surges in infection. This integrated fitting thus highlights the cumulative impact of successive epidemic waves and underscores the importance of maintaining continuous and adaptive public health measures to control the spread of COVID-19.

6. Optimal control problem

In this section, we examine the effect of implementing pharmaceutical and social interventions to reduce the outbreak of COVID-19. For this aim, we present a set of control variables $(u_1(t), u_2(t))$ where
(a) $u_1(t)$ implies the performance of vaccination continuously at time t.
(b) $u_2(t)$ implies treatment of quarantined individuals at time t.

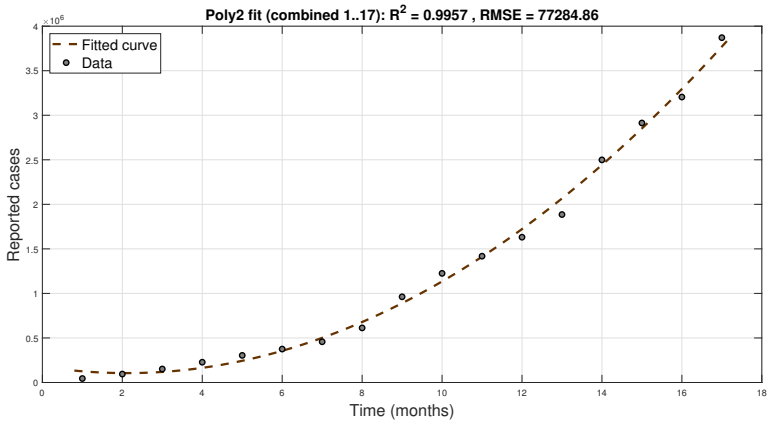

FIGURE 6. The observed monthly cumulative cases (for Iran) are approximated by a quadratic polynomial, from March 31, 2020 to July 31, 2021.

Thus, we reformulate the system (2.2) as an optimal control problem which is as follows:

$$\begin{aligned}
\frac{dS(t)}{dt} &= \rho - [\beta_s(1-\psi\xi)I_s(t) + \beta_a(1-\psi\xi)I_a(t)]S(t) - (\mu+u_1)S(t),\\
\frac{dV(t)}{dt} &= u_1 S(t) + \gamma R(t) - (1-\epsilon)\omega[\beta_s(1-\psi\xi)I_s(t) + \beta_a(1-\psi\xi)I_a(t)]V(t) - \mu V(t),\\
\frac{dE(t)}{dt} &= [\beta_s(1-\psi\xi)I_s(t) + \beta_a(1-\psi\xi)I_a(t)](S(t) + (1-\epsilon)\omega V(t)) - (\mu+\varphi)E(t),\\
\frac{dI_a(t)}{dt} &= \theta\varphi E(t) - (\alpha_a+\mu)I_a(t),\\
\frac{dI_s(t)}{dt} &= (1-\theta)\varphi E(t) - (\alpha_s+\mu)I_s(t),\\
\frac{dQ(t)}{dt} &= \eta\alpha_a I_a(t) + \sigma\alpha_s I_s(t) - (\mu+u_2)Q(t),\\
\frac{dR(t)}{dt} &= (1-\eta)\alpha_a I_a(t) + (1-\sigma)\alpha_s I_s(t) + u_2 Q(t) - (\mu+\gamma)R(t).
\end{aligned} \tag{6.1}$$

The main purpose of this study is to minimize the total infected individuals while reducing their relative costs. Hence, we construct the objective functional $J(u_1, u_2)$, which has to be minimized, where

$$J(u_1,u_2) = \int_0^T (A_1E + A_2I_a + A_3I_s + A_4Q + \frac{B_1}{2}u_1^2(t) + \frac{B_2}{2}u_2^2(t))dt. \tag{6.2}$$

Here, the costants A_i, $i = 1, ..., 4$ are respectively the per capita loss due to exist of exposed, asymptomatically infected, symptomatically infected and quarantined populations at any time instant. Moreover, the constants B_1 and B_2 represent the costs connected with vaccination of susceptible and treatment of quarantined individuals, respectively. We also take that the time interval is $[0, T]$. We seek optimal controls $u_1^\star(t)$ and $u_2^\star(t)$ satisfying

$$J(u_1^\star, u_2^\star) = min\{J(u_1,u_2), (u_1,u_2) \in U\},$$

where the control set U is

$$\begin{aligned}
U =&\{(u_1,u_2)|u_i(t) \text{ is Lebesgue measurable on } [0,1],\\
&0 \le u_i(t) \le 1 \text{ for all } t \in [0,T], i = 1,2\}.
\end{aligned}$$

6.1. **Characterization of optimal controls.** We will employ here Pontryagin's maximum principle [**?**] to search for the optimal controls that gratify the necessary conditions [**?**]. The Lagrangian for the optimal control problem is prescribed

$$L = A_1E + A_2I_a + A_3I_s + A_4Q + \frac{B_1}{2}u_1^2 + \frac{B_2}{2}u_2^2.$$

Now, we define the Hamiltonian H for the problem which is as follows

$$\begin{aligned}
H &= A_1E + A_2I_a + A_3I_s + A_4Q + \frac{B_1}{2}u_1^2 + \frac{B_2}{2}u_2^2 \\
&+ \lambda_1[\rho - [\beta_s(1-\psi\xi)I_s + \beta_a(1-\psi\xi)I_a]S - (\mu+u_1)S] \\
&+ \lambda_2[u_1S + \gamma R - (1-\epsilon)\omega[\beta_s(1-\psi\xi)I_s + \beta_a(1-\psi\xi)I_a]V - \mu V] \\
&+ \lambda_3[[\beta_s(1-\psi\xi)I_s + \beta_a(1-\psi\xi)I_a](S + (1-\epsilon)\omega V) - (\mu+\varphi)E] \\
&+ \lambda_4[\theta\varphi E - (\alpha_a+\mu)I_a] \\
&+ \lambda_5[(1-\theta)\varphi E - (\alpha_s+\mu)I_s] \\
&+ \lambda_6[\eta\alpha_aI_a + \sigma\alpha_sI_s - (\mu+u_2)Q] \\
&+ [(1-\eta)\alpha_aI_a + (1-\sigma)\alpha_sI_s + u_2Q - (\mu+\gamma)R].
\end{aligned}$$

where λ_i, $i = 1, 2, ..., 7$ are the adjoint variables satisfying the following adjoint system:

$$\begin{aligned}
\lambda_1' &= -\frac{\partial H}{\partial S} = (\lambda_1-\lambda_3)[\beta_s(1-\psi\xi)I_s + \beta_a(1-\psi\xi)I_a] + (\lambda_1-\lambda_2)u_1 + \lambda_1\mu, \\
\lambda_2' &= -\frac{\partial H}{\partial V} = (\lambda_2-\lambda_3)[(1-\epsilon)\omega[\beta_s(1-\psi\xi)I_s + \beta_a(1-\psi\xi)I_a] + \lambda_2\mu], \\
\lambda_3' &= -\frac{\partial H}{\partial E} = -A_1 + (\lambda_5-\lambda_4)\theta\varphi + (\lambda_3-\lambda_5)\varphi + \lambda_3\mu, \\
\lambda_4' &= -\frac{\partial H}{\partial I_a} = -A_2 + (\lambda_7-\lambda_6)\eta\alpha_a + (\lambda_4-\lambda_7)\alpha_a + \lambda_4\mu \\
&+ \beta_a(1-\psi\xi)[\lambda_1S + \lambda_2(1-\epsilon)\omega V - \lambda_3(S + (1-\epsilon)\omega V)], \\
\lambda_5' &= -\frac{\partial H}{\partial I_s} = -A_3 + (\lambda_7-\lambda_6)\sigma\alpha_s + (\lambda_5-\lambda_7)\alpha_s + \lambda_5\mu \\
&+ \beta_s(1-\psi\xi)[\lambda_1S + \lambda_2(1-\epsilon)\omega V - \lambda_3(S + (1-\epsilon)\omega V)], \\
\lambda_6' &= -\frac{\partial H}{\partial Q} = -A_4 + (\lambda_6-\lambda_7)u_2 + \lambda_6\mu, \\
\lambda_7' &= -\frac{\partial H}{\partial R} = (\lambda_7-\lambda_2)\gamma + \lambda_7\mu.
\end{aligned} \tag{6.3}$$

The transversality conditions (or boundary conditions) are

$$\begin{aligned}
&\lambda_1(T) = 0, \lambda_2(T) = 0, \lambda_3(T) = 0, \lambda_4(T) = 0, \\
&\lambda_5(T) = 0, \lambda_6(T) = 0, \lambda_7(T) = 0.
\end{aligned} \tag{6.4}$$

By the optimality condition, we have $\frac{\partial H}{\partial u_1} = 0$ and $\frac{\partial H}{\partial u_2} = 0$.

This implies, $B_1u_1 + (\lambda_2-\lambda_1)S = 0$ and $B_2u_2 + (\lambda_7-\lambda_6)Q = 0$. Thus, $u_1 = \frac{\lambda_1-\lambda_2}{B_1}S$ and $u_2 = \frac{\lambda_6-\lambda_7}{B_2}Q$.

Clearly,

$$\frac{\partial^2 H}{\partial u_1^2} = B_1 > 0,$$

$$\begin{vmatrix} \frac{\partial^2 H}{\partial u_1^2} & \frac{\partial^2 H}{\partial u_1 \partial u_2} \\ \frac{\partial^2 H}{\partial u_2 \partial u_1} & \frac{\partial^2 H}{\partial u_2^2} \end{vmatrix} = \begin{vmatrix} B_1 & 0 \\ 0 & B_2 \end{vmatrix} = B_1B_2 > 0.$$

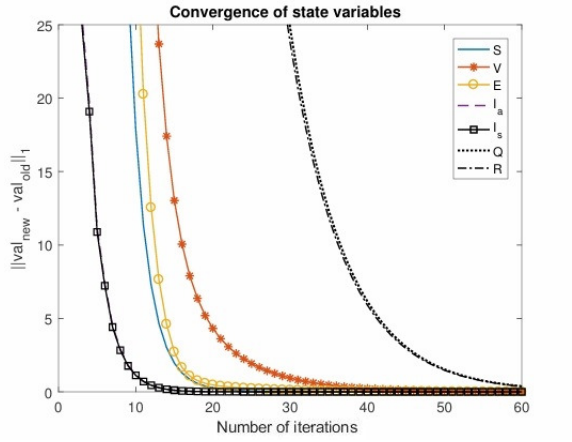

FIGURE 7. Convergence of state variables.

Finally, we get $u_1^\star = max\{0, min(1, \frac{(\lambda_1^\star - \lambda_2^\star)}{B_1} S^\star)\}$, $u_2^\star = max\{0, min(1, \frac{(\lambda_6^\star - \lambda_7^\star)}{B_2} Q^\star)\}$. Here, $S^\star$ and $Q^\star$ are the optimum values of S and Q and $(\lambda_1^\star, \lambda_2^\star, \lambda_3^\star, \lambda_4^\star, \lambda_5^\star, \lambda_6^\star, \lambda_7^\star)$ is the solution of the system (6.1) satisfying the conditions (6.4).

We solve (6.1) by utilizing forward-backward sweep method [**?**]. The time horizon for the optimal control problem was taken as the normalized interval ($[0, 1]$). This choice was made for mathematical convenience, as it corresponds to a rescaled version of the actual time horizon. Specifically, one unit of time in the simulations corresponds to one month, so that the interval ($[0, 1]$) represents a one-month period of intervention. Regarding the initial conditions, the susceptible and other compartment sizes were rescaled by dividing the actual population numbers by a large constant (10^5), in order to avoid numerical overflow and to simplify the computational implementation. Therefore, while the numerical values may appear small, they in fact represent proportions of the real population sizes. This rescaling does not affect the qualitative dynamics or the optimal control strategies, but makes the numerical analysis more tractable. We use the parametric values which are presented in Table **??** with $A_1 = A_2 = A_3 = A_4 = 1$, $B_1 = 1$, $B_2 = 1$, and initial conditions, $S(0) = 23$, $V(0) = 16$, $E(0) = 18$, $I_a(0) = 19$, $I_s(0) = 39$, $Q(0) = 5$, and $R(0) = 38$.

Figure 7 shows convergence of state variables $(S, V, E, I_a, I_s, Q, R)$ and it shows that the norm of each state variable tends to zero in each iteration. val_{new} is the vector of approximated values of each state variable during the current iteration and val_{old} is the vector of approximated values from the previous iteration. Here, $||.||$ implies to the ℓ^1 norm for vectors. This figure displays, $||val_{new} - val_{old}||_1$ converges to zero.

Figure 8 illustrates the influence of the vaccination control variable $u_1(t)$ on the COVID-19 dynamics governed by model (6.1). The simulation compares the temporal behavior of all state variables under two distinct scenarios: (i) without any intervention ($u_1(t) = 0$) and (ii) with the optimal vaccination strategy ($u_1(t) \neq 0$). As seen in the first subplot, the vaccinated population $V(t)$ increases sharply during the early phase of the intervention, indicating the immediate implementation of vaccination efforts. After reaching a peak, $V(t)$ stabilizes as the number of individuals eligible for vaccination decreases over time.

The exposed population $E(t)$ shows a clear reduction in the presence of vaccination, which reflects the direct effect of immunization in lowering the number of individuals who move from the susceptible to the exposed class. The sizes of the asymptomatically infected $I_a(t)$ and symptomatically infected $I_s(t)$ populations remain nearly unchanged with or without the vaccination control, suggesting that this intervention exerts little influence on these infection classes.

The quarantined population $Q(t)$ experiences an initial increase due to existing infections; however, there is negligible difference in the magnitude and temporal profile of $Q(t)$ between the controlled and uncontrolled scenarios. Meanwhile, the recovered population $R(t)$ increases steadily throughout the intervention period, however, there is negligible difference in the magnitude and temporal profile of $R(t)$ between the controlled and uncontrolled scenarios.

The time profile of the optimal control $u_1(t)$ reveals that the vaccination effort starts at its maximum intensity and then gradually declines to zero toward the end of the considered period. This pattern implies that the most effective

control policy is to apply a strong vaccination campaign at the beginning of the outbreak and subsequently reduce the effort as the epidemic becomes contained and the pool of unvaccinated individuals decreases.

Considering that the control variable u_2 is focused on the treatment of quarantined individuals, one could present its effect solely on the Q and R compartments. However, to confirm that this variable has no significant impact on the V through I_s compartments, these groups are also included in the results.

In Figure 9, panel (e) clearly demonstrates that the quarantined population $Q(t)$ is substantially lower when the treatment control is applied: with $u_2(t)$ active $Q(t)$ declines, whereas in the no-control case $Q(t)$ continues to increase during the simulation period. Accordingly, panel (f) shows a marked increase in the recovered population $R(t)$ under control, confirming that treatment expedites the transfer from quarantine to recovery. The control profile indicates a strong initial treatment effort (control near its upper bound) that is relaxed over time as the number of quarantined and infectious individuals diminishes. Overall, the results reveal that $u_2(t)$ primarily reduces the quarantined burden and accelerates recovery. Figures 8 and 9 indicate that each control, u_1 and u_2, alone is insufficient to reduce the populations of infected individuals such as Q, I_a, and I_s. The simultaneous application of both control variables is therefore essential to effectively curb the spread of COVID-19.

Figures 10-15 display the graphical representations of the simulations of the COVID-19 model as a function of time without control and with optimal control. Observing these graphical figures, we can say, implementing control interventions at the optimum level can help to prevent the outbreak of the disease as depicted by the drastical decrease in the population of individuals in the exposed and quarantined classes and an increased in the vaccinated and recovered classes.

Figure 16 illustrates the optimal time-dependent control profiles for vaccination ($u_1^\star(t)$) and treatment of quarantined individuals ($u_2^\star(t)$) over a one-month intervention horizon. As observed, both control variables start at their maximum admissible levels, reflecting the necessity of an intensive initial intervention to effectively curb the spread of the infection. The vaccination control $u_1^\star(t)$ (solid red curve) remains close to its upper bound during the early stage ($t < 0.4$ months) and then decreases gradually as the pool of susceptible individuals declines and the number of vaccinated individuals increases. This downward trend indicates that once a sufficient portion of the population becomes protected, the need for continued high-intensity vaccination diminishes. On the other hand, the treatment control $u_2^\star(t)$ (blue dashed curve) stays at its upper bound for a longer duration, until approximately $t = 0.9$ months, before rapidly declining to zero near the end of the simulation period. This behavior suggests that treatment efforts should be sustained throughout most of the intervention period to manage the quarantined population effectively, accelerating recovery and preventing further transmission. Overall, these results demonstrate that the optimal strategy consists of an early, aggressive vaccination phase followed by a prolonged treatment phase, both of which together minimize the number of infected and quarantined individuals while balancing implementation costs.

7. Numerical and graphical analysis of sensitivity and disease-free equilibrium stability

Now, we present a graphical illustration showing that the disease-free equilibrium point (X_{dfep}) is both locally and globally asymptotically stable. The local stability of the disease-free equilibrium, as stated in Theorem 4.1, is depicted in Figure 17. In this figure, the infective compartments (E, I_a, I_s, Q) gradually approach the disease-free equilibrium. This convergence occurs when the basic reproduction number satisfies $\mathcal{R}_0 < 1$, indicating that the infection cannot maintain itself in the population. In practical terms, this means that each infected individual spreads the disease to fewer than one person on average, emphasizing that interventions aimed at reducing transmission can effectively suppress the epidemic and lead to eradication.

The global stability of the disease-free equilibrium, as established in Theorem 4.2, is illustrated in Figure **??** using the parameter values from Table **??** with $\beta_a = \beta_s = 0.0001$ and $\mathcal{R}_0 = 0.42626$. Here, we consider three distinct sets of initial population sizes, and in all cases, the solution trajectories converge to the disease-free equilibrium (X_{dfep}). Each panel in Figure **??** displays the temporal dynamics of different epidemiological compartments, including exposed (E), asymptomatic infected (I_a), symptomatic infected (I_s), quarantined (Q), and recovered (R) populations. Global

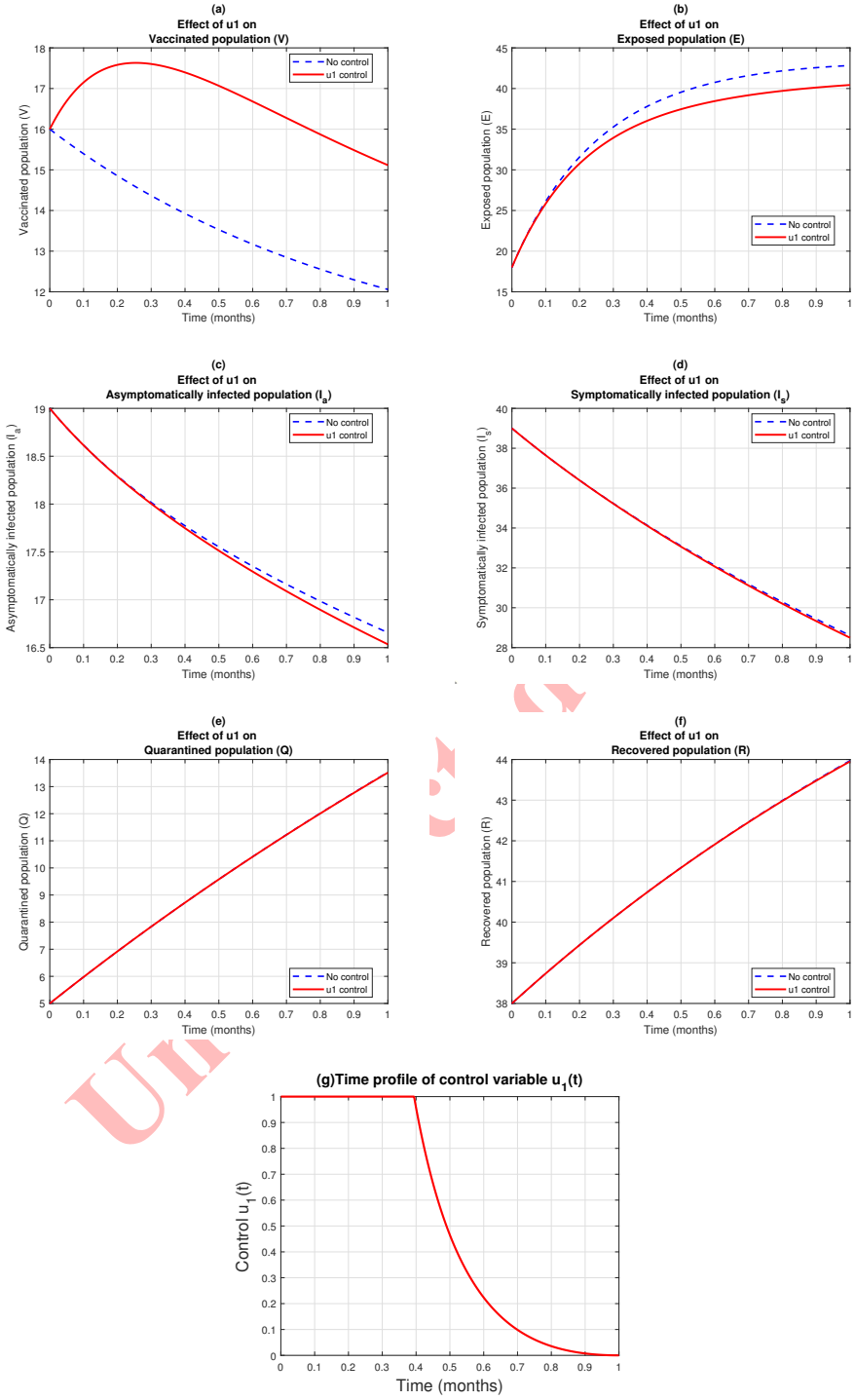

FIGURE 8. Effect of $u_1(t)$ (vaccination) on the COVID-19 dynamics governed by model (6.1).

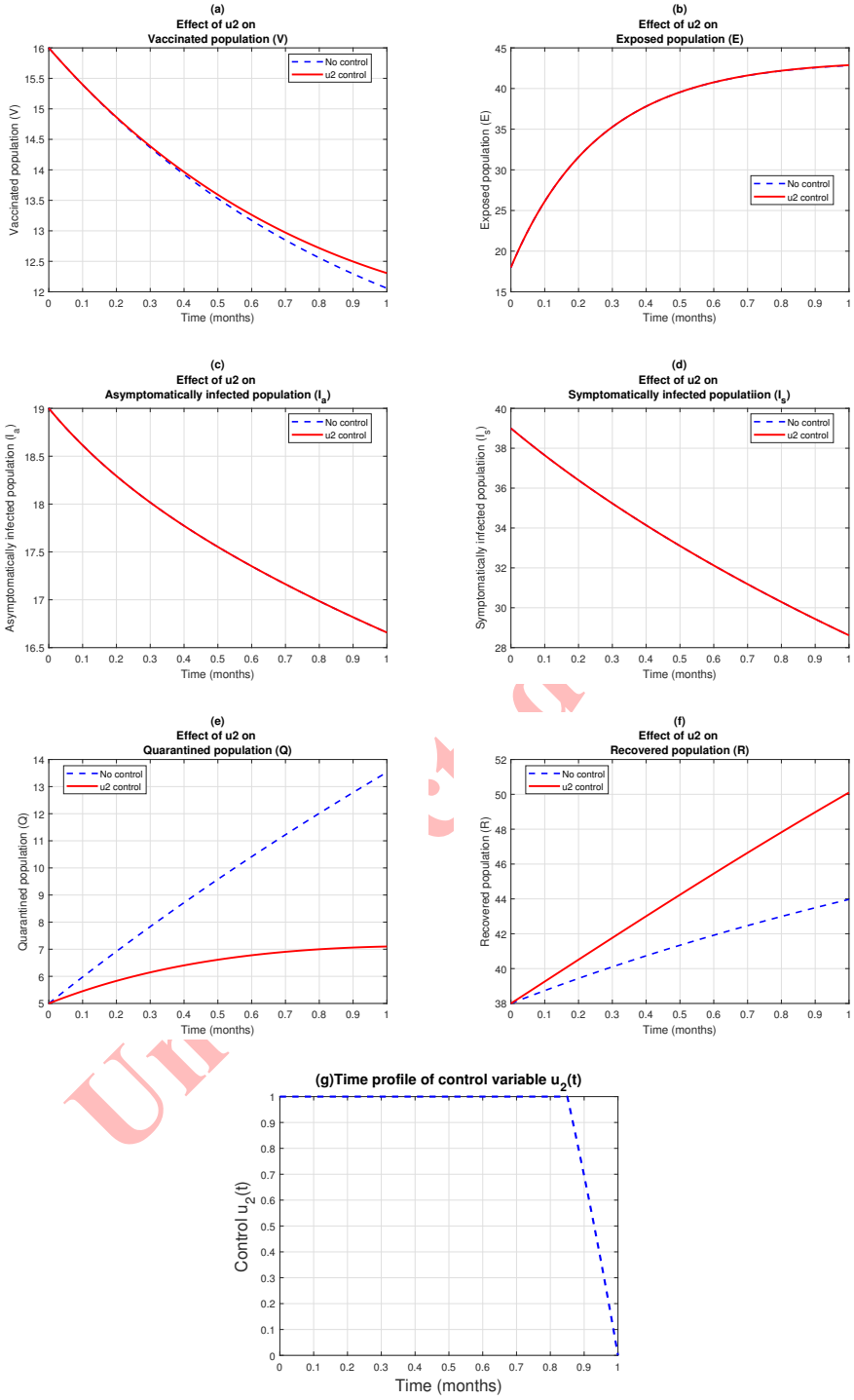

FIGURE 9. Effect of $u_2(t)$ (treatment of quarantined individuals) on the COVID-19 dynamics governed by model (6.1).

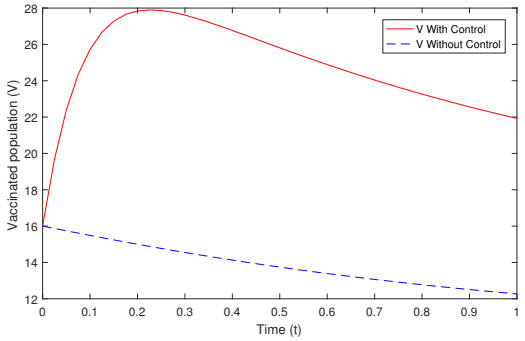

FIGURE 10. Dynamics of the vaccinated class with control and without control.

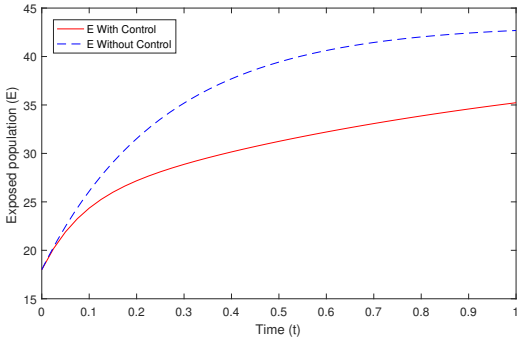

FIGURE 11. Dynamics of the exposed class with control and without control.

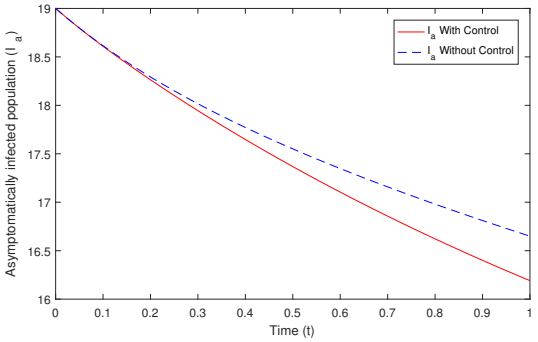

FIGURE 12. Dynamics of the asymptomatically infected class with control and without control.

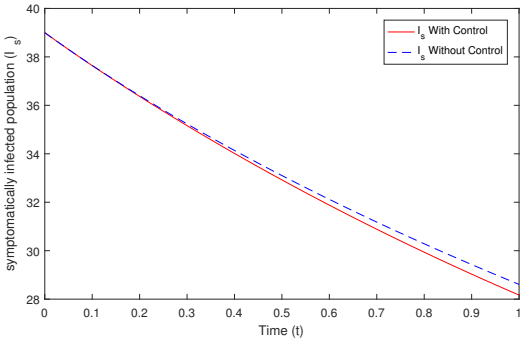

FIGURE 13. Dynamics of the symptomatically infected class with control and without control.

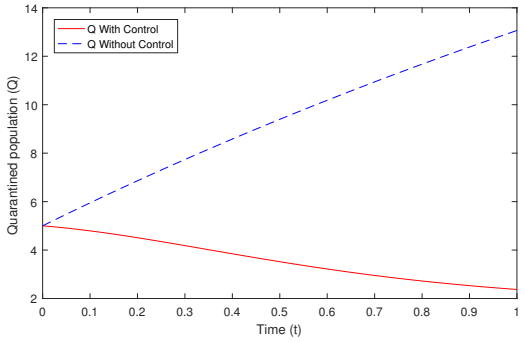

FIGURE 14. Dynamics of the quarantined class with control and without control.

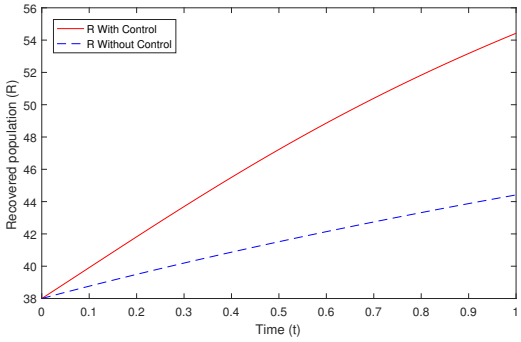

FIGURE 15. Dynamics of the recovered class with control and without control.

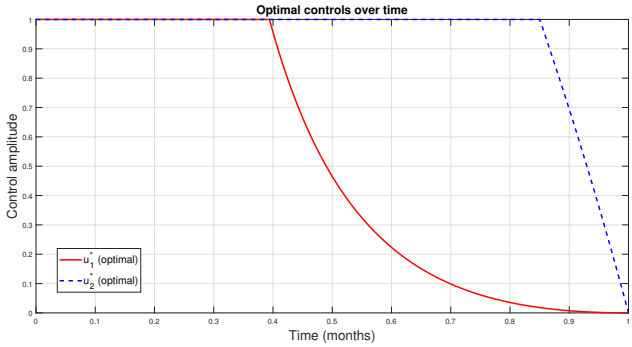

FIGURE 16. Optimal control trajectories for vaccination ($u_1^\star(t)$) and treatment of quarantined individuals ($u_2^\star(t)$) over the intervention period.

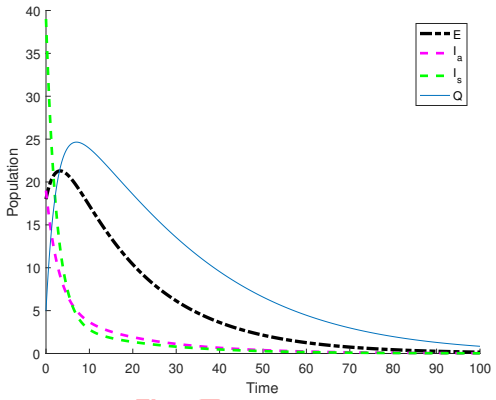

FIGURE 17. The local stability of DFEP for the model (2.2).

stability implies that the infection will eventually be eliminated regardless of the initial outbreak magnitude, reinforcing that sustained control measures can successfully lead to long-term eradication of COVID-19.

In order to find out how much a model is sensitive to changes in parameters, sensitivity analysis is used. It is derivable to the parameter x; the normalized forward sensitivity index is defined as follows:

$$\Upsilon_x^Y = \frac{x}{Y} \times \frac{\partial Y}{\partial x}. \tag{7.1}$$

The effective reproduction number $\mathcal{R}_0$ plays a significant role in predicting disease behavior. Therefore, we perform (7.1) to the parameters that $\mathcal{R}_0$ depends on. If the sensitivity index is positive, then it shows that $\mathcal{R}_0$ has a direct relationship with the parameter, and if it is negative, then it means it is inversely proportional to the parameter. According to what was expressed, $\mathcal{R}_0$ has a direct relationship with the parameters $x = \beta_a, \rho, \omega, \phi, \beta_s$ and it has an inverse relationship with the parameters $x = \psi, \xi, \epsilon, \mu, \alpha_a, \alpha_s$ and ν. It is not possible to give a definite opinion about the sign of $\Upsilon_\theta^{\mathcal{R}_0}$. The sensitivity indices evaluated at the parameter values are listed in Table **??** were written in Table **??**. Simulations for the model (2.2) is done using MATLAB $R2016b$ encoded with an $ODE45$ solver.

Figure **??** shows as α_a increases, the population of the asymptomatic infected compartment (I_a) decreases due to faster exit, while the quarantined population (Q) correspondingly increases due to higher transfer from I_a. This

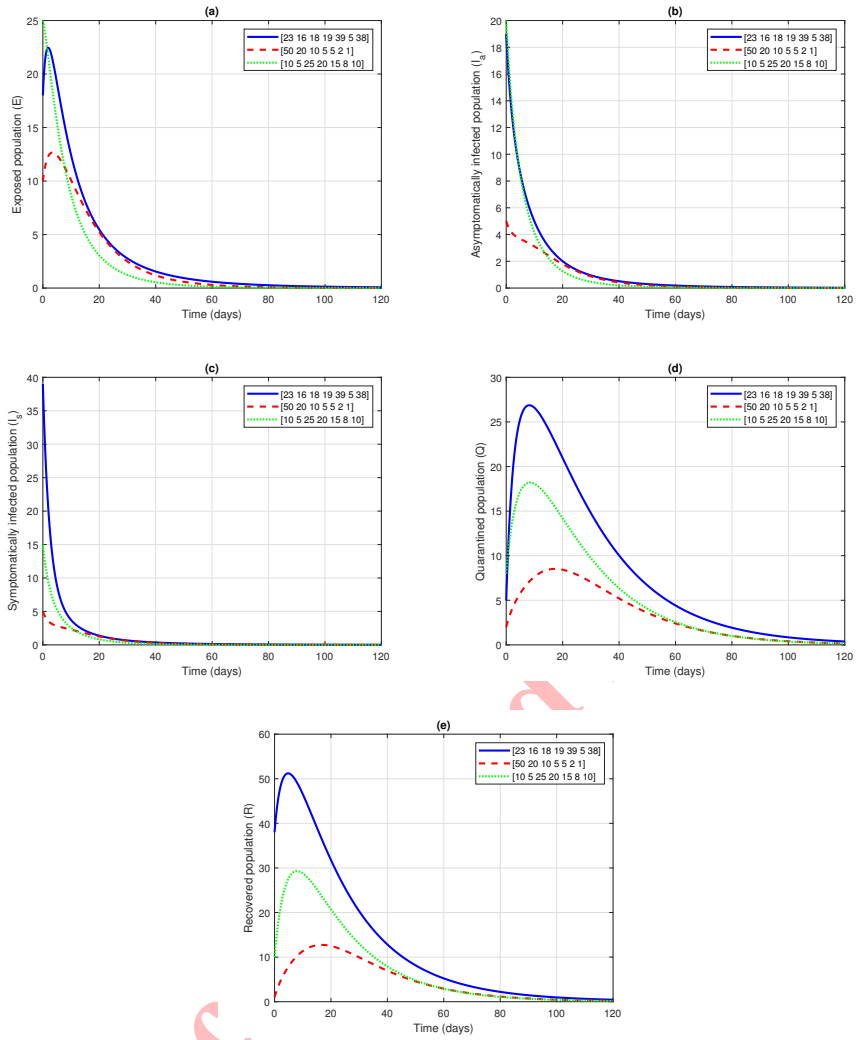

FIGURE 18. Convergence of solution trajectories for (a) exposed populations, (b) asymptomatic infected populations, (c) symptomatic infected populations, (d) quarantined populations, and (e) recovered populations starting from different initial values, using the parameter values from Table **??**, with $\beta_a = \beta_s = 0.0001$ and $\mathcal{R}_0 = 0.42626$.

indicates that enhancing the exit rate from asymptomatic infection, for example through timely detection and isolation, can reduce the spread of infection but simultaneously increases the quarantine burden, emphasizing the need for adequate quarantine resources.

As illustrated in Figure **??**, increasing the rate of immunity waning (γ) significantly affects the dynamics of all compartments. As γ increases, recovered individuals lose immunity more rapidly, returning to the susceptible pool and causing an increase in the exposed and infected populations (I_a and I_s). Consequently, the quarantined population (Q) also rises due to more detected infections. In contrast, the vaccinated (V) and recovered (R) populations decline over time as immunity fades. Overall, this figure highlights that higher values of γ sustain transmission and infection recurrence, emphasizing the importance of maintaining long-lasting immunity through booster vaccination strategies.

TABLE 6. Model parameter values and source.

Parameter	Value	Reference	Parameter	Value	Reference
ρ	0.35	Estimated	μ	3.6529×10^{-5}	[?]
β_s	0.01	Estimated	α_a	0.3	Estimated
ψ	0.1	[?]	η	0.1	Estimated
ξ	0.5	[?]	α_s	0.4	Estimated
β_a	0.2	Estimated	σ	0.6	Estimated
ν	0.05	Estimated	λ_q	0.05	[?]
ϵ	0.6	Estimated	γ	0.1	Estimated
ω	0.4	Estimated	$\mathcal{R}_0$	505	Calculated
φ	0.16	[?]	θ	0.5	[?]

TABLE 7. The normalized forward sensitivity indices of $\mathcal{R}_0$ to model parameters evaluated with the parameter values listed in Table **??**.

Parameters	Sensitivity indices	Values
β_a	$\Upsilon^{\mathcal{R}_0}_{\beta_a}$	0.963854
θ	$\Upsilon^{\mathcal{R}_0}_{\theta}$	0.927708
ρ	$\Upsilon^{\mathcal{R}_0}_{\rho}$	0.845410
β_s	$\Upsilon^{\mathcal{R}_0}_{\beta_s}$	0.036145
ω	$\Upsilon^{\mathcal{R}_0}_{\omega}$	0.009676
ϕ	$\Upsilon^{\mathcal{R}_0}_{\phi}$	0.000228
ν	$\Upsilon^{\mathcal{R}_0}_{\nu}$	−0.976923
α_a	$\Upsilon^{\mathcal{R}_0}_{\alpha_a}$	−0.963737
ξ	$\Upsilon^{\mathcal{R}_0}_{\xi}$	−0.052631
ψ	$\Upsilon^{\mathcal{R}_0}_{\psi}$	−0.052631
ϵ	$\Upsilon^{\mathcal{R}_0}_{\epsilon}$	−0.050441
α_s	$\Upsilon^{\mathcal{R}_0}_{\alpha_s}$	−0.036142

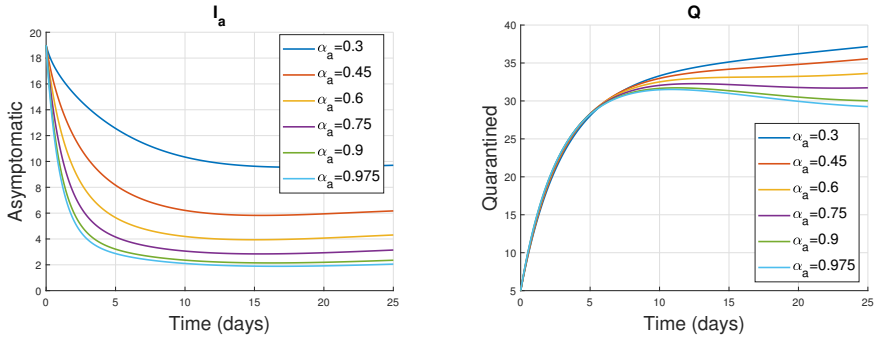

FIGURE 19. Solution curves depicting the impact of α_a on I_a and Q compartments of the model (2.2).

As shown in Figure **??**, increasing the recovery rate of quarantined individuals (λ_q) leads to a noticeable decline in the quarantined population (Q), since individuals recover and leave isolation more rapidly. Consequently, the

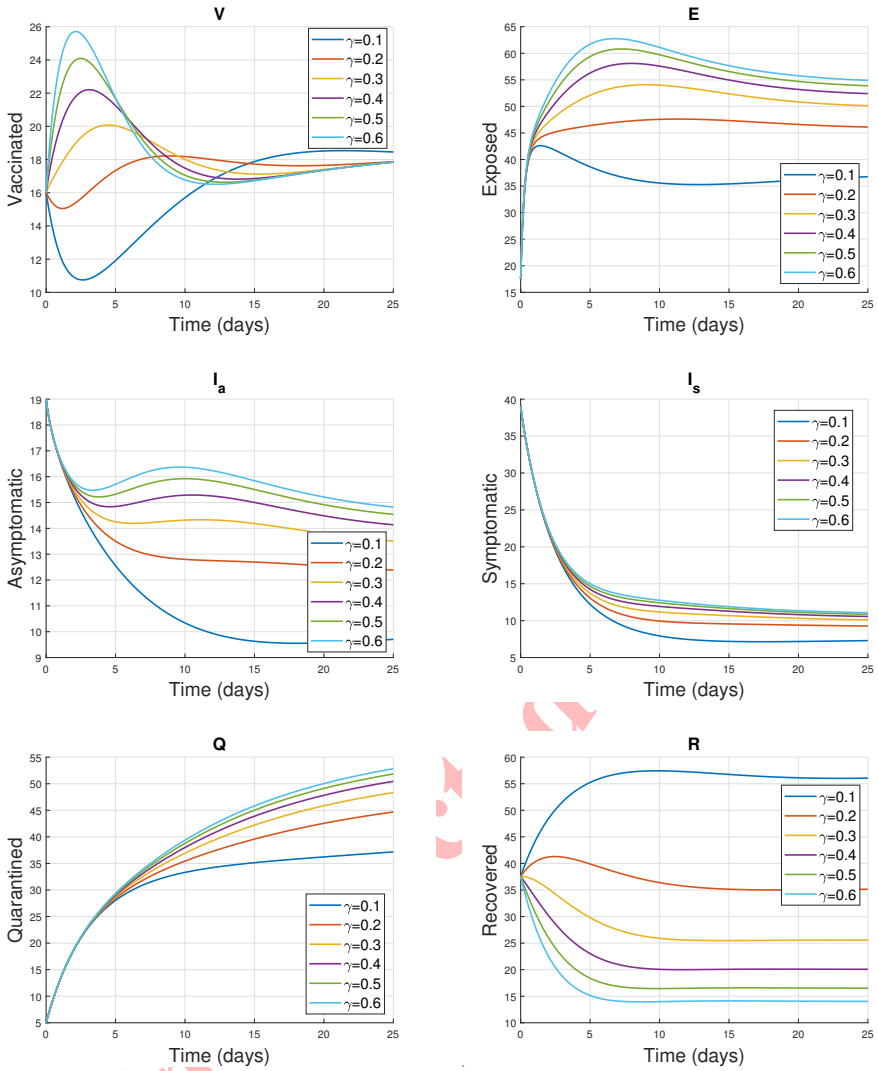

FIGURE 20. Solution curves depicting the impact of γ on V, E, I_a, I_s, Q, and R compartments of the model (2.2).

recovered population (R) increases due to the faster transition of individuals from quarantine to recovery. Moreover, for lower values of λ_q, the Q compartment accumulates more individuals and stabilizes at a higher level, while the R compartment reaches a smaller steady state. These results imply that enhancing the recovery rate within quarantine not only reduces the burden on isolation facilities but also accelerates the overall recovery process in the population, contributing to epidemic control and faster return to normal conditions.

Figure **??** shows that increasing the proportion of individuals wearing face masks (ψ) reduces the number of exposed (E), asymptomatic (I_a), and symptomatic (I_s) infections. This occurs because mask usage lowers the effective transmission rate ($1 - \psi\xi$), keeping more individuals in the susceptible class (S) uninfected. The figure highlights that even moderate increases in mask compliance can significantly slow the epidemic and reduce both detectable and undetectable transmissions. Figure **??** shows that increasing the proportion of symptomatic individuals who are quarantined (σ) reduces the number of active symptomatic infections (I_s) while increasing the quarantined (Q) and

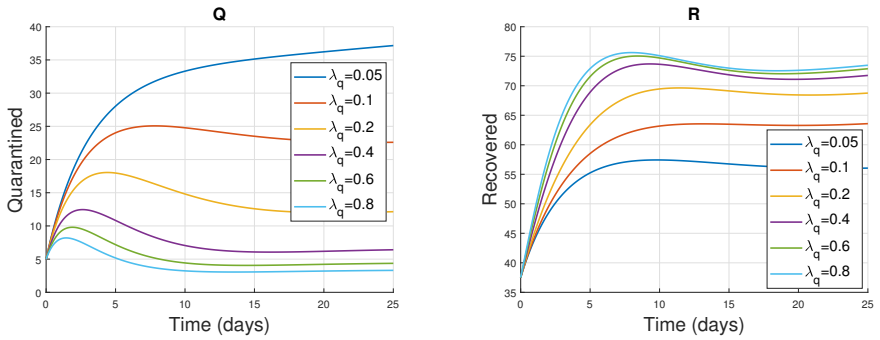

FIGURE 21. Solution curves depicting the impact of λ_q on Q and R compartments of the model (2.2).

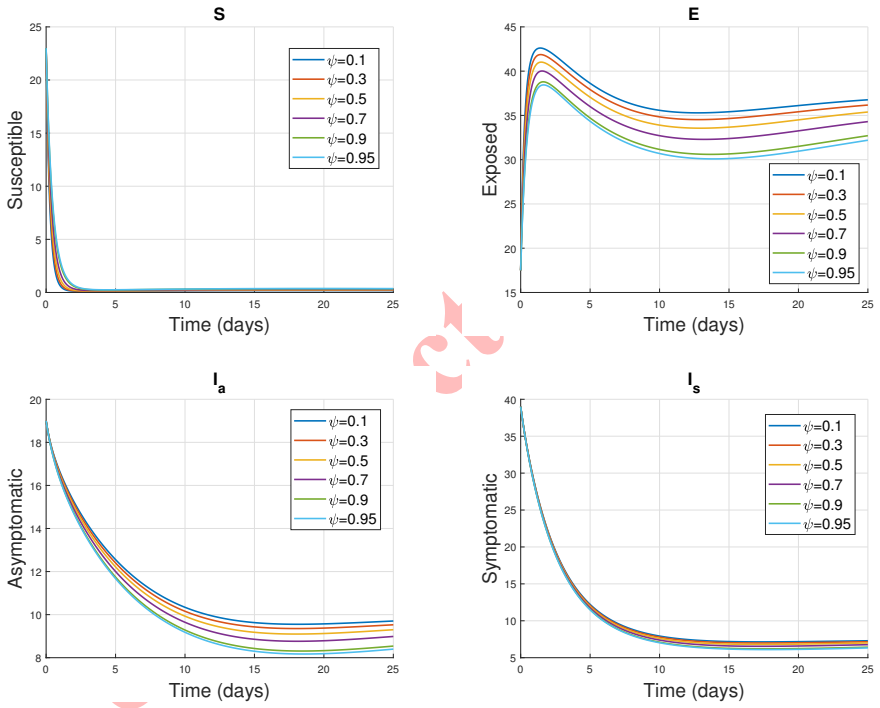

FIGURE 22. Solution curves depicting the impact of ψ on S, E, I_a, and I_s compartments of the model (2.2).

recovered (R) populations. This demonstrates that higher quarantine compliance effectively slows the epidemic and promotes recovery.

Furthermore, the contour plots of the effective basic reproduction number $\mathcal{R}_0$ for some of the parameters in model (2.2) are displayed in Figures **??**–**??** to investigate the effect of the intervention parameters on $\mathcal{R}_0$.
In Figure **??**, the contour shows that increasing the proportion of individuals who use a face mask reduces the amount of the basic reproduction number $\mathcal{R}_0$.

In addition, in Figure **??**, we have seen that increasing the efficacy of face masks reduces the amount of the basic reproduction number $\mathcal{R}_0$, but this is not sufficient to prevent the spread of COVID-19. From our sensitivity analysis,

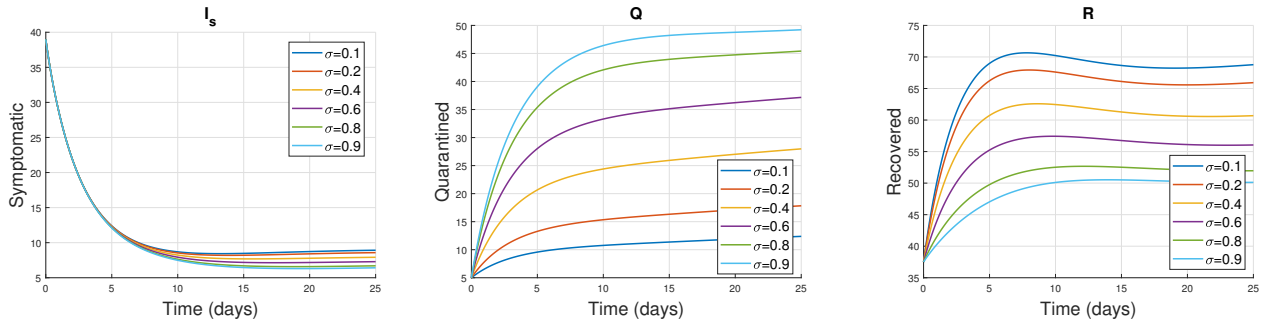

FIGURE 23. Solution curves depicting the impact of σ on I_s, Q, and R compartments of the model (2.2).

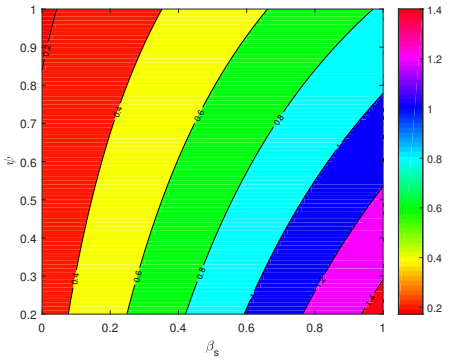

FIGURE 24. Contour plots of $\mathcal{R}_0$ versus the effective transmission rate from symptomatic infected class (β_s) and the proportion of individuals who use a face mask (ψ).

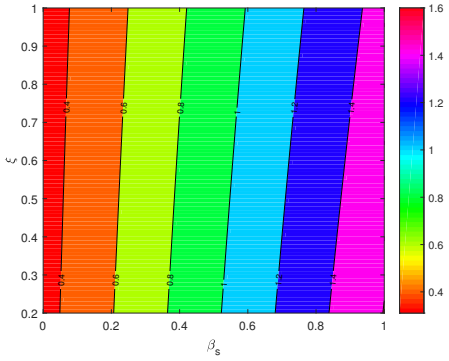

FIGURE 25. Contour plots of $\mathcal{R}_0$ versus the effective transmission rate from symptomatic infected class (β_s) and the efficacy of face masks (ξ).

we realized that the basic reproduction number $\mathcal{R}_0$ is the most sensitive to the parameters β_a, ω, ϕ, α_a, and ν.

In Figure **??**, the contour plots illustrate the combined influence of the vaccination rate (ν) and the effective transmission rate from symptomatic infected class (β_s) on the effective basic reproduction number, $\mathcal{R}_0$. As observed, $\mathcal{R}_0$ declines substantially with increasing ν, indicating that higher vaccination coverage effectively reduces disease transmission potential in the population. In contrast, $\mathcal{R}_0$ increases with increasing β_s, showing that higher transmissibility of the virus amplifies infection spread. The curved contour lines highlight the nonlinear relationship between these parameters: at low β_s, moderate vaccination can suppress the outbreak below the epidemic threshold ($\mathcal{R}_0 < 1$), whereas at higher β_s values, even strong vaccination efforts may not be sufficient to control the infection. This demonstrates the importance of maintaining both high vaccine uptake and interventions that reduce the effective transmission rate (such as mask usage and social distancing).

Figure **??**, displays the variation of $\mathcal{R}_0$ with respect to the effective transmission rate from symptomatic infected class (β_s). It can be seen that $\mathcal{R}_0$ increases with an increase in the effective transmission rate.

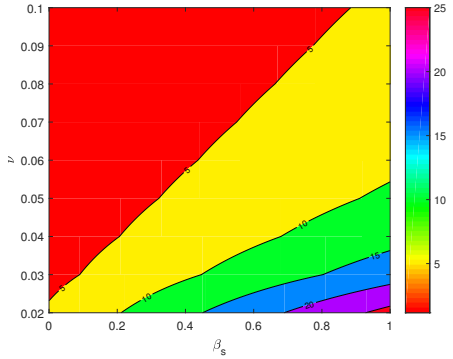

FIGURE 26. Contour plots of $\mathcal{R}_0$ versus the effective transmission rate from symptomatic infected class (β_s) and the vaccination rate (ν).

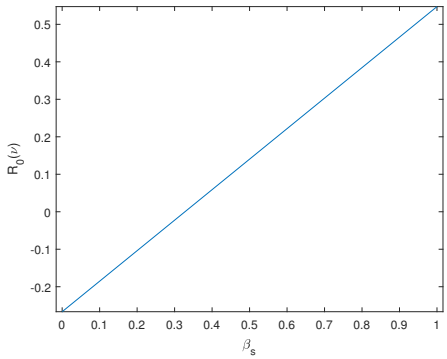

FIGURE 27. Variation of $\mathcal{R}_0$ with respect to the effective transmission rate β_s.

8. Conclusion

In this paper, we formulated and analyzed a mathematical model for the transmission dynamics of COVID-19. We obtained both disease-free and endemic equilibria for our model. Then, the basic reproduction number ($\mathcal{R}_0$) was computed using the next-generation matrix method. The local stability of the $DFEP$ has been proved by using the Jacobian matrix and Routh–Hurwitz criteria. Then, It was shown by utilizing the Lyapunov function that the disease-free equilibrium is globally asymptotically stable whenever $\mathcal{R}_0 < 1$. The local asymptotic stability of the endemic equilibrium is inferred through linearization around the equilibrium point, although explicit eigenvalue analysis is not carried out. The monthly reported COVID-19 cases in Iran from March 31, 2020, to July 31, 2021 were fitted with quadratic polynomial models, and the goodness of fit was assessed using R^2 and RMSE. We formulated an optimal control problem for the COVID-19 transmission model and solved it analytically using Pontryagin's Maximum Principle and numerically via the forward-backward sweep method. The main objective was to minimize the number of positive cases, including the exposed, asymptomatically infected, symptomatically infected, and quarantined populations. Our simulations revealed that vaccination alone significantly reduced the exposed population and gradually increased the vaccinated and recovered compartments, while the treatment of quarantined individuals primarily accelerated recovery and reduced the quarantined population. However, applying each control individually was insufficient to effectively suppress the spread of infection. The simultaneous implementation of both vaccination and treatment strategies provided the most effective reduction in infected populations while optimizing the associated costs. These results highlight the importance of early and intensive vaccination campaigns complemented by sustained treatment efforts for quarantined individuals in controlling the outbreak of COVID-19. Finally, sensitivity analysis confirmed that by increasing the vaccination rate (ν), increasing the proportion of symptomatic individuals who have been quarantined (σ), and increasing the proportion of individuals who use a face mask (ψ) will help to prevent the spread of the COVID-19 virus.

Funding

This research did not receive any specific grant from the funding agencies in the public, commercial, or not-for-profit sectors.

Declarations

Conflict of interest: Authors have no conflict of interest.

References

[1] https://ada.com/covid/covid-19-incubation-period.

[2] B. Agusto, N. Marcus, and O. Okosun, *Application of optimal control to the epidemiology of malaria*, Electronic Journal of Differential Equations, *81* (2012), 1-22.

[3] B. Agusto and R. Ogunye, *Avian influenza optimal seasonal vaccination strategy*, ANZIAM J, *51* (2010), 394-405.

[4] I. Ahmed, G.U. Modu, A. Yusuf, P. Kumam, and I. Yusuf, *A mathematical model of coronavirus disease (COVID-19) containing asymptomatic and symptomatic classes*, Results Phys, *21* (2021), 103776.

[5] T. Alqahtani, *Mathematical model of SIR epidemic system (COVID-19) with fractional derivative: stability and numerical analysis*, Advances in Difference Equations a Springer open Journal, (2021), 2.

[6] Attaullah and M. Sohaib, *Mathematical modeling and numerical simulation of HIV infection model*, Results in Applied Mathematics, *7* (2020).

[7] C. A. Beauchemin and A. Handel, *A review of mathematical models of influenza A infections within a host or cell culture: lessons learned and challenges ahead*, BMC Public Health, (2011), p. 15.

[8] C. Bowman, B. Gumel, P. V. Driessche, J. Wu, and H. Zhu, *A mathematical model for assessing control strategies against West Nile Virus*, Bulletin of Mathematical Biology, *67*(5) (2005), 1107-1133.

[9] J. Carr, *Applications Centre Manifold Theory, Springer-Verlog*, New York, (1981).

[10] C. Castillo-Chavez and B. Song, *Dynamical models of tuberculosis and their application*, Math Biosci Eng, *1* (2004): 361-404.

[11] https://www.cdc.gov/coronavirus/2019-ncov/your-health/isolation.html.

[12] M. L. Diagne, H. Rwezaura, S. Y. Tchoumi, and J. M. Tchuenche, *A mathematical model of COVID-19 with vaccination and treatment*, Computational and mathematical methods in medicine, (2021).

[13] P. V. Driessche and J. Watmough, *Reproduction numbers and sub-threshold endemic equilibria for compartmental models of disease transmission*, Mathematical biosciences, *180*(1-2) (2002), 29-48.

[14] M. Erfanian, M. Gachpazan, and H. Gholami, *A mathematical model of Chikungunya transmission incorporating a fear parameter and a chronic-outcome variable*, Mathematical research, (2026).

[15] A. Fehr and S. Perlman, *Coronaviruses: An overview of their replication and pathogenesis*, Springer Science + Business Media, New York, (2015).

[16] H. Gholami, M. Gachpazan, and M. Erfanian, *An efficient mathematical model for the Outbreak of COVID-19 from the perspective of numerical analysis*, Iraqi Journal of Science, *66* (2025), 5124-5135.

[17] H. Gholami, M. Gachpazan, and M. Erfanian, *A three-layered compartmental model of Nipah virus transmission with analysis*, Journal of Mathematical Modeling, *13* (2025), 445-466.

[18] H. Gholami, M. Gachpazan, M. Erfanian, and M. Hasanzadeh, *An analytical modeling framework for breast cancer progression and treatment evaluation*, Healthcare Analytics, *9* (2026).

[19] H. Gholami, M. Gachpazan, M. Erfanian, and M. Hasanzadeh, *Mathematical modeling of breast cancer: Analyzing immune-chemotherapy interactions and sensitivity to key parameters*, Advances in Cancer Biology-Metastasis, *16* (2026).

[20] H. Gholami, M. Gachpazan, and M. Erfanian, *Mathematical modeling and dynamic analysis of dengue fever: examining economic and psychological impacts and forecasting disease trends through 2030—a case study of Nepal*, Scientific Reports, *15* (2025).

[21] H. Gholami, M. Gachpazan, and M. Erfanian, *SEI_aI_sQRS epidemic model for COVID-19 by using compartmental analysis and numerical simulation*, Computational Methods for Differential Equations, *13* (2025), 592-607.

[22] J. K. Ghosh, S. K. Biswas, S. Sarkar, and U. Ghosh, *Mathematical modelling of COVID-19: A case study of Italy*, Mathematics and computers in simulation, (2022).

[23] M. Heidari, N. Sayfouri, and H. Jafari, *Consecutive Waves of COVID-19 in Iran: Various Dimensions and Probable Causes*, Disaster Medicine and Public Health Preparedness, (2022).

[24] X. He, E. H. Y. Lau, P. Wu, and et al., *Temporal dynamics in viral shedding and transmissibility of COVID-19*, Nature, *26* (2020), 672-675.

[25] Johns Hopkins University Coronavirus Resource Center, Coronavirus cases- Iran, Available from: https://www.indexmundi.com/coronavirus/country/ir.

[26] E. Jung, S. Lenhart, and Z. Feng, *Optimal control of treatments in a two-strain tuberculosis model*, Discrete and Continuous Dynamical Systems-Series B, *2* (2002), 473-482.
[27] S. Lenhart and J. T. Workman, *Optimal control applied to biological model*, mathematical and computational biology series Chapman and Hall/CRC, (2007).
[28] Y. Li and J. S. Muldowney, *On Bendixson's criterion*, J Differ Equ, *106*(1) (1993), 27–39.
[29] R. Li, S. Pei, B. Chen, and et al, *Substantial undocumented infection facilitates the rapid dissemination of novel coronavirus (SARS-CoV-2)*, Science, *368* (2020), 489-493.
[30] M. Mandal, S. Jana, S. K. Nandi, A. Khatua, S. Adak, and T. K. Kar, *A model based study on the dynamics of COVID-19: Prediction and control*, Chaos, Solitons & Fractals, *136* (2020).
[31] S. D. D. Njankou and F. Nyabadza, *Modelling the role of human behavior in Ebola virus disease (EVD) transmission dynamics*, Computational and Mathematical Methods in Medicine, (2022).
[32] M. Parsamanesh and M. Erfanian, *Global dynamics of an epidemic model with standard incidence rate and vaccination strategy*, Chaos, Solitons and Fractals, *117* (2018), 192-199.
[33] M. Parsamanesh, M. Erfanian, and S. Mehrshad, *Stability and bifurcations in a discrete-time epidemic model with vaccination and vital dynamics*, BMC Bioinformatics, *21* (2020).
[34] M. Parsamanesh and M. Erfanian, *Stability and bifurcations in a discrete-time SIVS model with saturated incidence rate*, Chaos, Solitons & Fractals, *150* (2021).
[35] L. S. Pontryagin, V. G. Boltyanskii, R. V. Gamkrelidze, and E. F. Mishchenko, *The mathematical theory of optimal processes*, Wiley, New Jersey, (1962).
[36] P. Riyapan, S. F. Shuaib, and A. Intarasit, *A mathematical model of COVID-19 pandemic: A case study of Bangkok, Thailand*, Computational and Mathematical Methods in Medicine, (2021).
[37] A. K. Suhuyini and B. Seidu, *A mathematical model on the transmission dynamics of typhoid fever with treatment and booster vaccination*, Frontiers in Applied Mathematics and Statistics, *9* (2023).
[38] D. A. Tyrrell, *Cultivation of a novel type of common-cold virus in organ cultures*, British Medical Journal, *1* (1965), 1467-1470.
[39] J. M. Visy, P. L. Coz, B. Chadefaux, C. Fressinaud, F. Woimant, J. Marquet, J. Zittoun, J. Visy, J. M. Vallat, and M. Haguenau, *Homocystinuria due to 5,10- methylenetetra-hydrofolate reductase deficiency revealed by stroke in adult siblings*, Neurology, *41* (1991), 1313-1315.
[40] H. C. Wei, *Mathematical modeling of ER-positive breast cancer treatment with AZD9496 and palbociclib*, AIMS mathematics, (2020).
[41] X. Yan, Y. Zou, and J. Li, *Optimal quarantine and isolation strategies in epidemics control*, World Journal of Modelling and Simulation, *3* (2007), 202-211.